THE ASTROPHYSICAL JOURNAL, 472:54–72, 1996 November 20

RADIO RECOMBINATION LINES FROM THE NUCLEAR REGIONS OF STARBURST GALAXIES

JUN-HUI ZHAO
Institute of Astronomy and Astrophysics, Academia Sinica, P.O. Box 1-87, Taipei, Taiwan 115; and Harvard-Smithsonian Center for Astrophysics, 60 Garden Street, MS 78, Cambridge, MA 02138

K. R. ANANTHARAMAIAH
Raman Research Institute, Bangalore 560 080, India

W. M. GOSS
National Radio Astronomy Observatory, P.O. Box O, Socorro NM 87801

AND

F. VIALLEFOND
DEMIRM, Observatoire de Meudon, F-92190 Meudon, France
Received 1996 January 4; accepted 1996 June 5

ABSTRACT

Using the Very Large Array (VLA) with an angular resolution of 3″, we have detected the hydrogen recombination line H92α from the galaxies Arp 220, M83, and NGC 2146. The line emission arises from the nuclear regions with a line-to-continuum ratio of 1% or less.

In order to fit both the observed H92α line and continuum data in the nuclear regions, we have considered two types of models. First, we utilize a model with a collection of H II regions. A large number of compact H II regions are required in this model. With electron temperatures in the range 5×10^3–1×10^4 K and a range of electron densities, this model can account for both the line intensity and the continuum spectrum. In most cases, the H92α line is dominated by internal stimulated emission due to free-free continuum arising within the H II regions. In a low-density case ($n_e = 50$ cm^{-3}) for Arp 220, about half the line emission comes from external stimulated emission due to the background nonthermal source. Typical rates of ionizing photons predicted from these models are $\sim 5 \times 10^{52}$ s^{-1} for M83, $\sim 4 \times 10^{53}$ s^{-1} for NGC 2146, and 5×10^{54} s^{-1} for Arp 220. We infer that 10^5 O5 stars are required in Arp 220, which is an order of magnitude greater than in NGC 2146 and 2 orders of magnitude greater than in M83. Alternatively, several uniform slab models with $T_e \geq 5 \times 10^3$ and n_e in the range of 50–1×10^4 cm^{-3} appear to fit both the H92α line and continuum data of Arp 220 and M83. In the low-density models, stimulated emission by the background nonthermal radiation appears to be dominant at low frequencies, and the lines at higher frequencies arise primarily from spontaneous emission. The uniform slab model requires a higher ionizing photon rate than the H II region model. No slab models with reasonable T_e can fit the data observed in M83 and NGC 2146.

Combining previous published data with these new observations, a sample of 13 galaxies has been observed for radio recombination lines (RRLs) with the VLA. Nine out of the 13 galaxies have been detected in the H92α line. While the H92α line luminosity appears to be correlated with the Brα line luminosity, we find that nearly all the RRL galaxies show a significant excess in H92α line compared to the expected LTE value. The excess in the H92α line flux suggests that non-LTE effects are important for the H92α line in these starburst nuclei. A strong correlation between H92α and the molecular lines of HCN/HCO$^+$ is also found, indicating that the RRL emitters may be spatially associated with the dense molecular cores. The inferred high electron density also suggests an intimate relation between the RRLs and the dense molecular medium in these galaxies.

Subject headings: galaxies: nuclei — galaxies: starburst — galaxies: stellar content — radio lines: galaxies

1. INTRODUCTION

Radio recombination lines (RRLs) have been demonstrated to be a useful tool in the study of ionized gas in external galaxies (e.g., Shaver 1978; Roelfsema & Goss 1992; Anantharamaiah et al. 1993). The dominant sources of RRLs on a galactic scale are the H II regions associated with young OB stars; thus, these lines are excellent diagnostics of present star formation. In addition, since RRLs are not affected by extinction, it is possible to determine the physical conditions (electron temperature, electron density, kinematics, and the geometry of ionized gas distribution) in the nuclear region of external galaxies. This type of study has been pursued successfully in extragalactic systems by Anantharamaiah & Goss (1990) for NGC 253, Puxley et al. (1991) for NGC 2146, and Seaquist, Kerton, & Bell (1994) for M82.

Recent detections of the H92α line from NGC 1365, NGC 3628, and IC 694 show a promising future in studying extragalactic RRLs with the Very Large Array (VLA)[1] (Anantharamaiah et al. 1993, hereafter Paper I). The observations of RRLs from the starburst galaxies can be used to constrain models of the nuclei of these systems. The

[1] The VLA is a facility of the National Radio Astronomy Observatory (NRAO). The NRAO is a facility of the National Science Foundation, operated under cooperative agreement by Associated Universities, Inc.

interpretation of the line emission depends upon the geometry, physical condition, and line emission mechanism; these can be determined by observations of both the line and continuum emission at a number of frequencies if the angular resolution is better than several arcseconds. In Paper I, we have suggested that the H92α lines in nearby normal galaxies are produced mainly by the spontaneous and stimulated emission due to the continuum emission from the source itself. However, the stimulated lines due to strong background nonthermal radiation may be important in some cases, and the stimulating mechanism may help detection of RRLs from distant galaxies and quasi-stellar objects. (QSOs) as suggested by Shaver (1978). Further RRL observations in a larger sample covering more distant galaxies are required.

In this paper, we describe new observations of the H92α line in Arp 220, M83, NGC 2146, and NGC 6240 in § 2. New detections of the H92α line are discussed in § 3. We discuss several models constrained by the available line and continuum data in § 4. Finally, in § 5, the observed H92α line intensity is compared with existing Brα and HCN/HCO^+ observations. $H_0 = 75$ km s^{-1} Mpc^{-1} is assumed.

2. OBSERVATIONS AND DATA REDUCTION

The H92α line observations of the galaxies Arp 220, M83, NGC 2146, and NGC 6240 were made during 1992 February to April using the VLA in the C configuration with a typical angular resolution of 3″. The rest frequency of the H92α line is 8309.384 MHz. In all the observations, a VLA spectral line mode with 15 channels was used, covering a bandwidth of 25 MHz or a velocity coverage of $\sim$900 km s^{-1}. The frequency resolution is 1.56 MHz (or 57 km s^{-1}). Each source was observed for about 7 hours. The observing parameters are summarized in Table 1. Columns (1)–(3) give the names and positions of the galaxies, respectively. The heliocentric velocity defined as $V_{\rm Hel} = [(\lambda - \lambda_0)\lambda_0^{-1}]c$ is given in column (4), where λ is redshifted wavelength and λ_0 are the rest wavelengths of the H92α line. Columns (5) and (6) list both the calibrators for correcting the complex gains of the VLA system, and the calibrators used to determine the frequency response (bandpass) of the instrument. The date of the observation is given in column (7), and the configuration is given in column (8). The flux density scale of the observations was set by observing the radio source 3C 286. On-line Hanning smoothing was applied.

The continuum data were obtained by averaging the central 13 channels. Further phase corrections for the continuum data were obtained using a self-calibration procedure. These phase corrections were also applied to each of the line channels. Continuum emission superimposed on the line was subtracted utilizing the UVLIN algorithm (Cornwell, Uson, & Haddad 1992). Line images have been made for these data using natural weighting in order to achieve optimal sensitivity. Typical rms noise in each channel image is about 90 μJy beam^{-1}.

3. RESULTS

3.1. *New Detections of* H92α *Line emission*

The H92α line was detected in Arp 220, M83, and NGC 2146. Spectra obtained by integrating over the line emission region are shown in Figures 1*a*–1*c*. The line was not detected in NGC 6240. Some relevant characteristics of these galaxies are noted below.

3.2. *Notes to Individual Sources*

3.2.1. *Arp 220*

Arp 220 (=IC 4553) is a prototypical ultraluminous far-infrared (FIR) galaxy (the FIR luminosity exceeds 1×10^{12} $L_\odot$; Emerson et al. 1984). The FIR luminosity is usually interpreted in terms of thermal emission from heated dust grains, although it has been debated whether a burst of massive star formation or an embedded quasar is the dominant heating source (e.g., Solomon & Sage 1988; Sanders et al. 1988).

In the optical, a double-lobed structure is observed, arising from an opaque dust screen crossing the true nucleus (Joy et al. 1986). The presence of a double nuclear source with a separation of 1″ at both radio and infrared wavelengths suggests that the activity may have been initiated by a recent merger (Norris 1988; Graham et al. 1990).

A large central molecular mass concentration was revealed in high-resolution CO observations, indicating a high surface molecular density (Scoville et al. 1991). A large visual extinction ($A_V \sim 1000$ mag) was inferred in the direction of the nucleus based on the inferred molecular hydrogen column density. CS emission was also detected at 144.3 GHz, indicating the presence of about 10^{10} $M_\odot$ of molecular gas with densities of $n_{\rm H_2} \approx 10^5$ cm^{-3} (Solomon, Radford, & Downes 1990).

A very broad H I absorption (743 km^{-1}) was observed with an H I column density of $N_{\rm H\,I} = 1.1 \times 10^{20}$ T_s cm^{-2} (Mirabel 1982). VLA H I observations reveal a large velocity gradient of the H I–absorbing gas across the nuclear disk (Baan et al. 1987).

The OH megamasers from the nuclear region were discovered by Baan, Wood, & Haschick (1982) and were imaged with VLBI techniques by Diamond et al. (1989) and Lonsdale et al. (1994). The latter group showed that the OH line in Arp 220 originates in a structure ≤ 1 pc that is superimposed on a compact component of the nuclear contin-

TABLE 1

OBSERVING PARAMETERS OF RRL (H92α) OBSERVATIONS WITH THE VLA

Galaxy (1)	α(1950) (2)	δ(1950) (3)	$V_{\rm Hel}$[a] (km s^{-1}) (4)	ϕ Calibrator (5)	Bandpass Calibrator (6)	Observation Date (7)	Configuration (8)
Arp 220.....	15 32 46.88	23 40 07.9	5551	1600+335	3C 286	1992 Feb 23	C
M83.....	13 34 11.12	−29 36 41.7	511	1336−260	3C 286	1992 Apr 17	C
NGC 2146.....	06 10 41.10	78 22 28.1	852	0615+820	3C 286	1992 Feb 23	C
NGC 6240.....	16 50 27.83	02 28 58.5	7535	1655+077	3C 286	1992 Feb 25	C

NOTE.—Units of right ascension are hours, minutes, and seconds; units of declination are degrees, arcminutes, and arcseconds.

[a] $V_{\rm Hel} = [(\lambda - \lambda_0)/\lambda_0]c$, where c is the light speed.

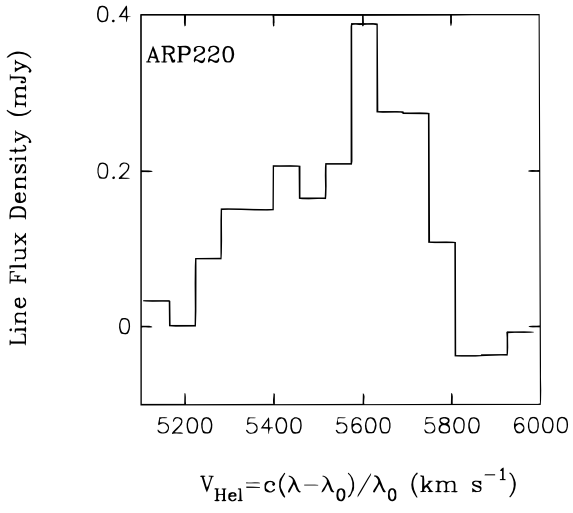

FIG. 1*a*

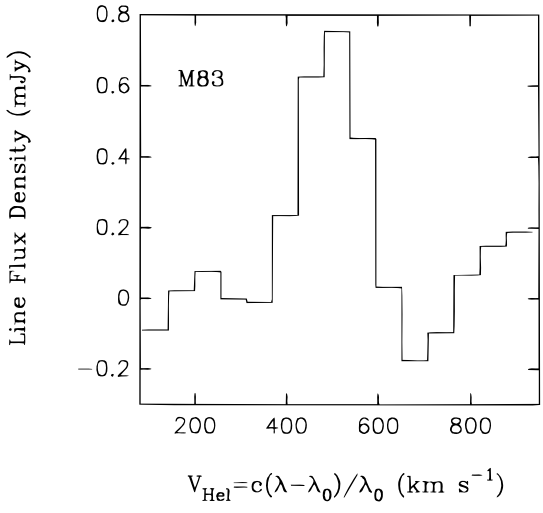

FIG. 1*b*

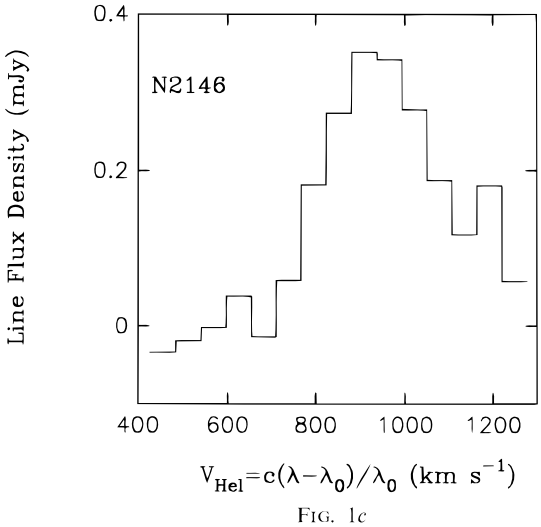

FIG. 1*c*

FIG. 1.—H92α spectra integrated over the line emission region for the galaxies (*a*) Arp 220; (*b*) M83; (*c*) NGC 2146

uum emission. These results suggest that much of the FIR radiation arises in a dense molecular torus surrounding a possible quasar.

The H92α line is detected toward the nucleus of Arp 220 (Fig. 2*a*). The integrated line profile is broad with ΔV(FWHM) = 320 km s^{-1} (Fig. 1*a*). The intensity-weighted mean systemic velocity of V_{Hel} = 5560 km s^{-1} is 140 km s^{-1} greater than that determined in the H I absorption observations (Baan et al. 1987). In Figure 2*b*, both the blueshifted (5240–5522 km s^{-1}) and redshifted H92α (5522–5804 km s^{-1}) line emission features are imaged and are overlain on the radio continuum image at 1.3 cm with a resolution of 0".1 (Norris 1988). The line emission centroid in the blueshifted image shows a significant displacement from the redshifted component, which is coincident with the nuclear continuum component. This displacement suggests the presence of a velocity gradient from higher velocity in the northeast to a lower velocity in the southwest. This velocity gradient is consistent with H I, CO, and CS observations (Baan et al. 1987; Scoville et al. 1991; Radford et al. 1991).

3.2.2. *M83*

M83 (NGC 5236) is a nearly face-on, SBc/SBb type galaxy. Along the spiral arms, there are a number of nonthermal and thermal radio components that were identified as supernova remnants and H II regions (Cowan & Branch 1985). A compact nuclear source was found with a spectral index of $\alpha = -0.5$ (Ondrechen 1985; Cowan & Branch 1985).

Both CO and C^+ lines were found from the central region of the galaxy (Rickard et al. 1977; Crawford et al. 1985). The CO emission was imaged using the 45 m telescope at Nobeyama (Handa et al. 1990). The CS line emission was also detected toward the nucleus (Mauersberger et al. 1989). Detection of both Brα and Brβ lines were reported by Turner, Ho, & Beck (1987).

Puxley et al. (1991) searched for the H53α and H40α lines toward this galaxy. The derived upper limits to the line flux densities are 26 and 170 mJy (3 σ). The H92α line has been detected from this galaxy. The line emission region is spatially resolved, and the peak line intensity is less than 2.5 σ

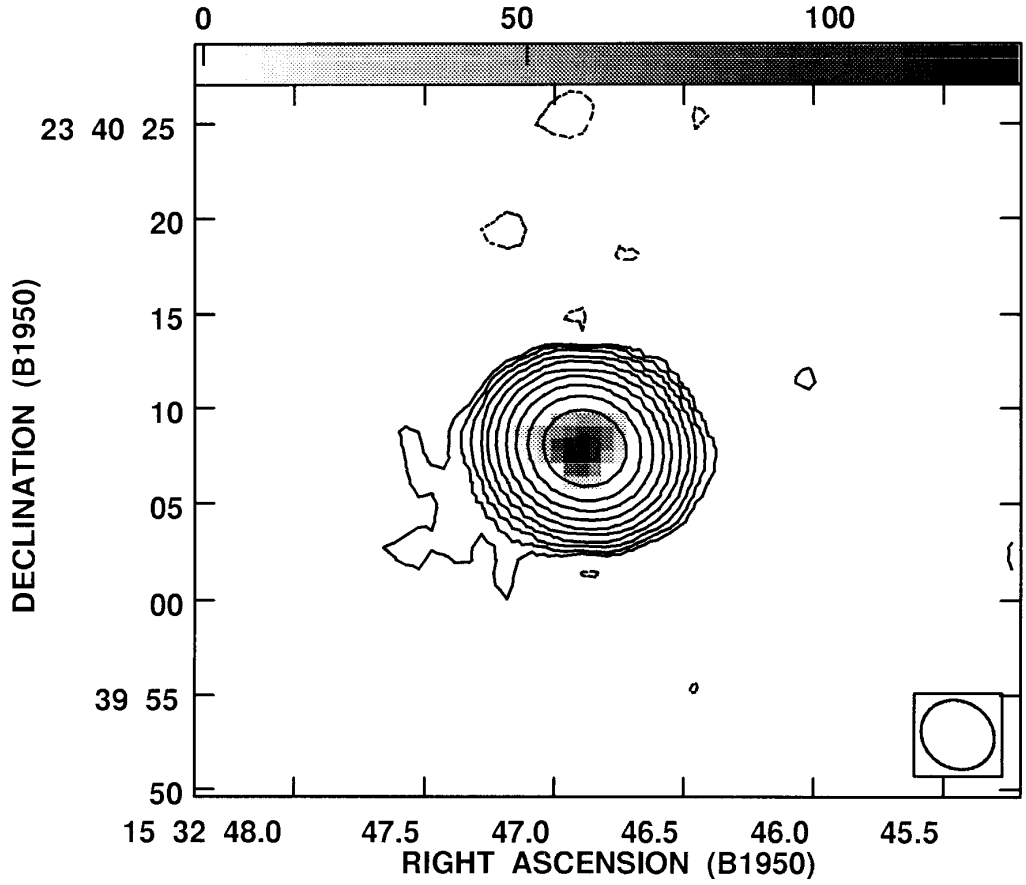

FIG. 2a

FIG. 2.—(*a*) Continuum image of Arp 220 at 8.2 GHz made with natural weighting; beam (FWHM) = 4.″0 × 3.″5 (P.A. = 56°). Contours are −0.12, 0.12, 0.24, 0.48, 0.96, 1.92, 3.84, 7.68, 15.4, 30.7, 61.4, and 122.9 mJy beam^{-1}. The gray-scale representation, with a range of line flux 0–125 mJy beam^{-1} km s^{-1}, indicates the H92α line emission. (*b*) The H92α line emission at 5240–5522 km s^{-1} and 5523–5804 km s^{-1}. Contours are 12, 17, 24, 34, 48, and 69 mJy beam^{-1} km^{-1}. The gray scale represents the continuum images at 22.5 GHz with a flux density range of 0.8–5 mJy beam^{-1}.

(1 σ = rms). The line profile integrated over the central region shows a significant peak line intensity (S/N > 5) and a rather narrow line width (FWHM = 95 km s^{-1}). Such narrow line profile is also found from the observations of CO, C^+, and CS in the nucleus of M83 (Sanders & Mirabel 1985; Crawford et al. 1985; Mauersberger et al. 1989). Figure 3*a* shows the H92α line region overlain on the continuum image at 8.3 GHz. Much of the line emission is distributed to the southeast of the continuum peak but is extended in the north-south direction. This extension of the H92α line appears to be consistent with the CO emission in the central region (see Handa et al. 1990). A velocity gradient of about 8 km s^{-1} per arcsecond (660 km s^{-1} per kpc) is shown in the position-velocity diagram made along the north-south direction (Fig. 3*b*). The velocity structure with higher velocity to the south and lower velocities to the north is consistent with that observed in CO.

3.2.3. *NGC 2146*

NGC 2146 is a somewhat edge-on (inclination angle = 51°; Young et al. 1988), nearby peculiar spiral galaxy. The central regions of NGC 2146 are highly optically obscured by dust lanes along the disk (e.g., Hutchings et al. 1990). The galaxy is also a powerful far-infrared source. Surrounding NGC 2146, an enormous H I halo (extent of 150 kpc) was discovered by Fisher & Tully (1976), although the origin of the H I gas remains uncertain. Observations of CO at millimeter wavelengths show a large concentration of molecular gas in the central 30″ (2 kpc) (Jackson & Ho 1988; Young et al. 1988). With an angular resolution of 7″, Young et al. (1988) observed the CO kinematics with a regular progression from 1050 km s^{-1} in the northwest to 700 km s^{-1} in the southeast. Recently, Puxley et al. (1991) detected the H53α line at 43 GHz from this galaxy.

The galaxy has strong radio continuum emission associated with an inner 3 kpc disk (Kronberg & Biermann 1981). Figure 4*a* shows a noticeable asymmetric structure in extended continuum emission of the galactic disk. The excess emission southwest of the disk is obvious. The S shape of the central continuum emission ridge is formed by three relatively compact components as observed at higher resolutions (1″) at 6 cm (Kronberg & Biermann 1981). The average spectral index of the continuum emission between 20 and 6 cm within the central 36″ is about −0.5 ($S \propto \nu^{\alpha}$). Two of the central triple sources were detected at 2 cm with a resolution of 0.″19 × 0.″14; the compact radio emission can be explained as the result of star formation (Carral, Turner, & Ho 1990).

The H92α line was detected from the nuclear region (Fig. 4*b*). A position-velocity diagram along the major axis is shown in Figure 4*c*. A velocity gradient of 70 km s^{-1} per

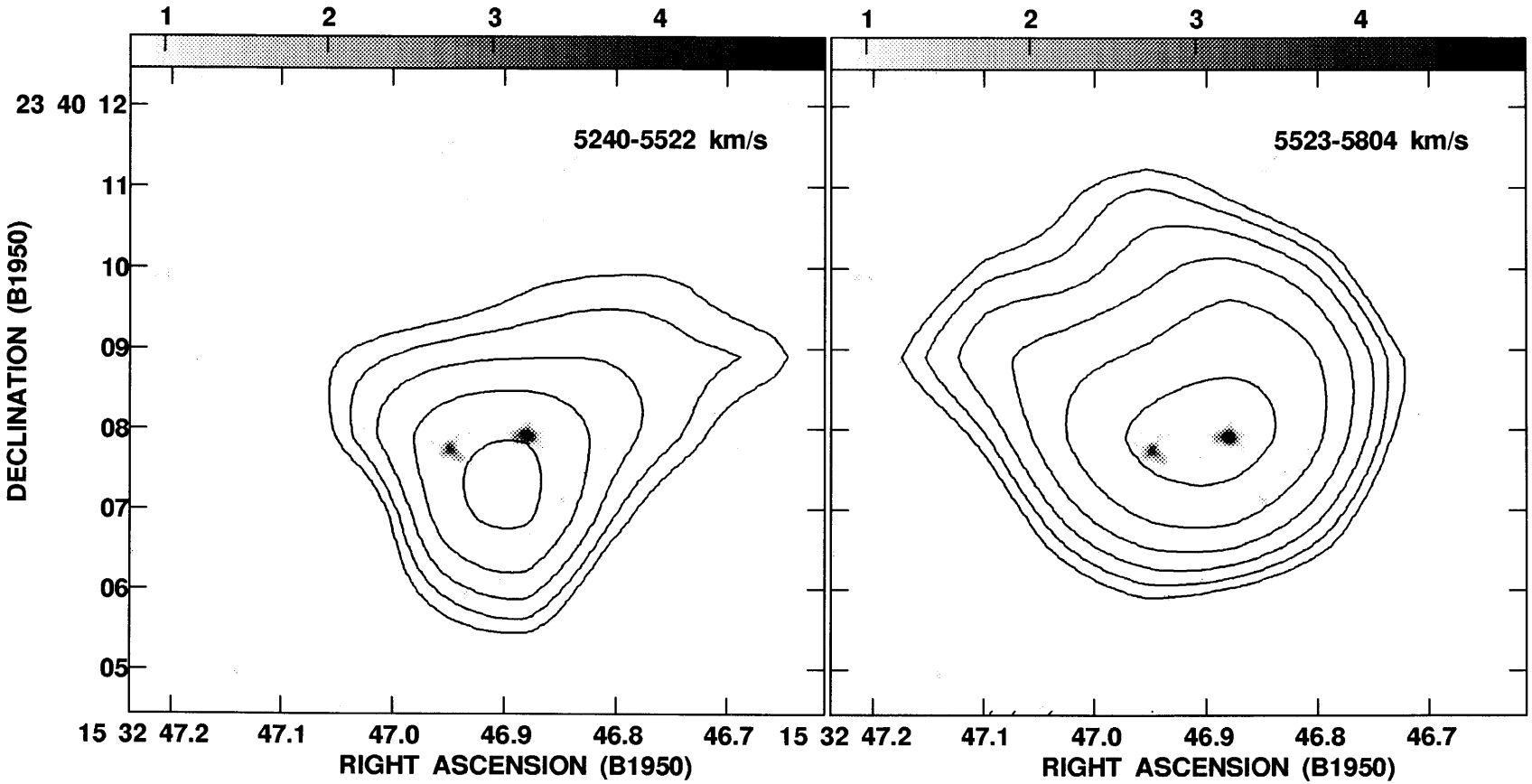
1
2
3
4
5240-5522 km/s
5523-5804 km/s
DECLINATION (B1950)
23 40 12
11
10
09
08
07
06
05
15 32 47.2
47.1
47.0
46.9
46.8
46.7
RIGHT ASCENSION (B1950)

FIG. 2*b*

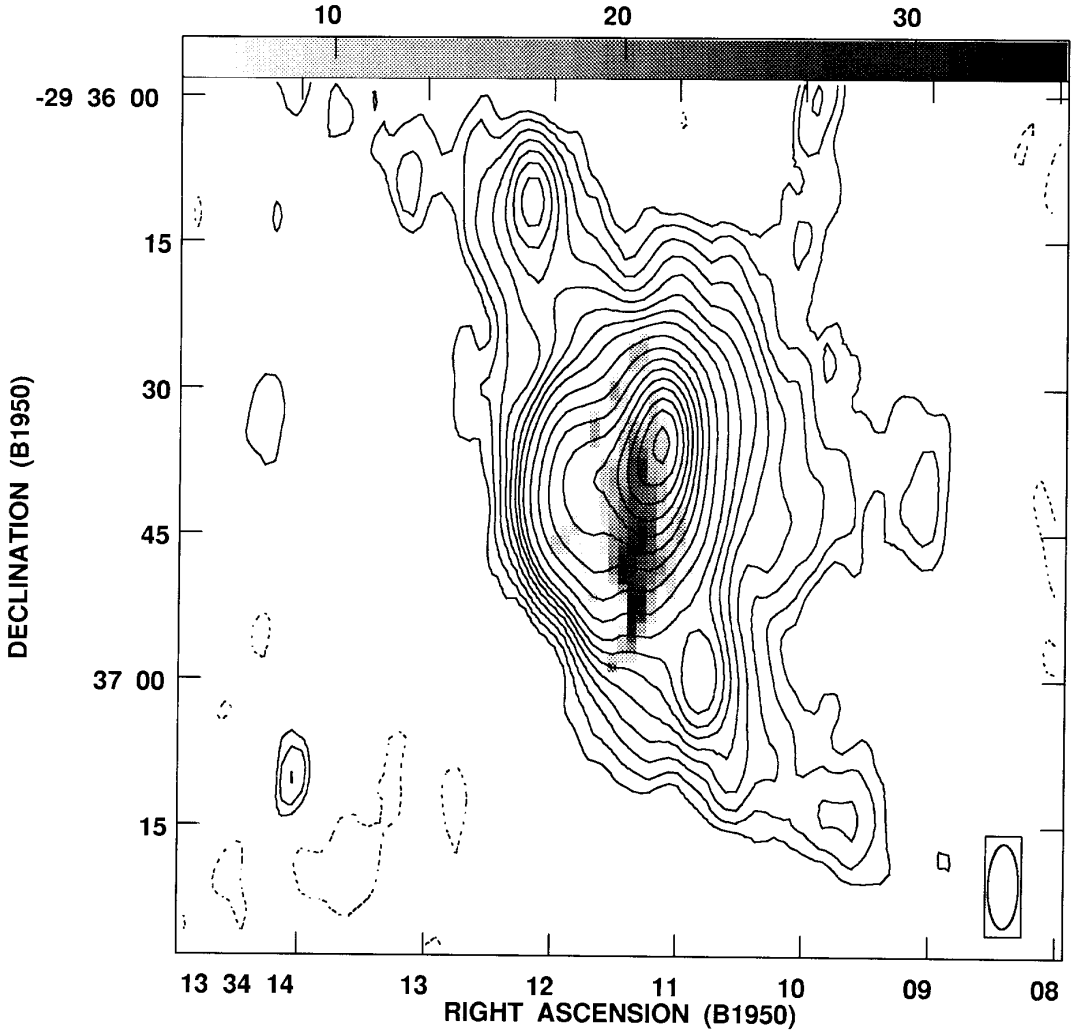

FIG. 3a

FIG. 3.—(*a*) Continuum image of M83 at 8.3 GHz made with natural weighting. Contours are −0.14, 0.11, 0.18, 0.28, 0.42, 0.60, 0.81, 1.1, 1.4, 2.1, 3.2, 4.6, 6.3, 8.4, 11, 14, 17, and 21 mJy beam^{-1}. The beam size (FWHM) is 8.″7 × 3.″1 (P.A. = −1°). The gray-scale representation, with a range of line flux 5–35 mJy beam^{-1} km s^{-1}, indicates the H92α line emission. (*b*) Position-velocity diagram taken along declination (left is north, and right is south). The reference position is $\alpha(1950) = 13^h34^m11^s.01$, $\delta(1950) = -29°36'41''.7$. Contours are −0.09, 0.06, 0.09, 0.12, 0.15, 0.18, 0.21, 0.24, and 0.27 mJy beam^{-1}. The cross indicates the resolution in both velocity and position coordinates.

arcsecond (or 900 km s^{-1} kpc^{-1}) is observed with higher velocities in the northwest and lower velocities to the southeast. The nuclear kinematic structure is consistent with that observed in CO (Young et al. 1988) and suggests that the H92α emission arises in the rotating nuclear disk.

3.3. *Upper Limit in NGC 6240*

In many aspects, NGC 6240 has the same characteristics as Arp 220. Its distorted optical morphology along with double nucleus observed at radio and infrared (Eales et al. 1990) suggests a recent galaxy merger. CO observations show a concentration of molecular gas in the nucleus (Wang, Scoville, & Sanders). On the basis of the low ratio of Brα luminosity to FIR luminosity, Depoy, Becklin, & Wynn-Williams (1986) pointed out that the FIR emission may be powered by a hidden quasar.

NGC 6240 is the most distant galaxy observed in the H92α line. Figure 5 shows the continuum image observed at 8.1 GHz. No significant H92α line emission was detected from this galaxy. The 3 σ upper limit in the H92α line flux density is 0.27 mJy beam^{-1}, corresponding to an integrated flux of 2.1×10^{-23} W m^{-2} assuming $\Delta V_{\rm FWHM} = 250$ km s^{-1}.

3.4. *Summary of the* H92α *Line Measurements*

In Table 2, the results of the H92α observations are summarized for the four galaxies. We list the positions of the radio continuum peak. For the detected galaxies, we determine the peak line flux density integrated over the region in which the line was detected. The quoted errors for the peak line flux density are dominated by the rms noise in each channel image. For nondetections, we give 3 σ upper limits. The integrated line flux densities presented in Table 2 are determined by integrating the line intensity over both the line emission region and the velocity channels with a cutoff of 3 σ. The central heliocentric velocity and the FWHM velocity width are determined from a Gaussian fit to each integrated spectrum in Figure 1.

3.5. *Continuum Flux Density from the* H92α *Emission Region*

For NGC 2146, M83, and Arp 220, the continuum flux densities from the RRL emission regions were determined

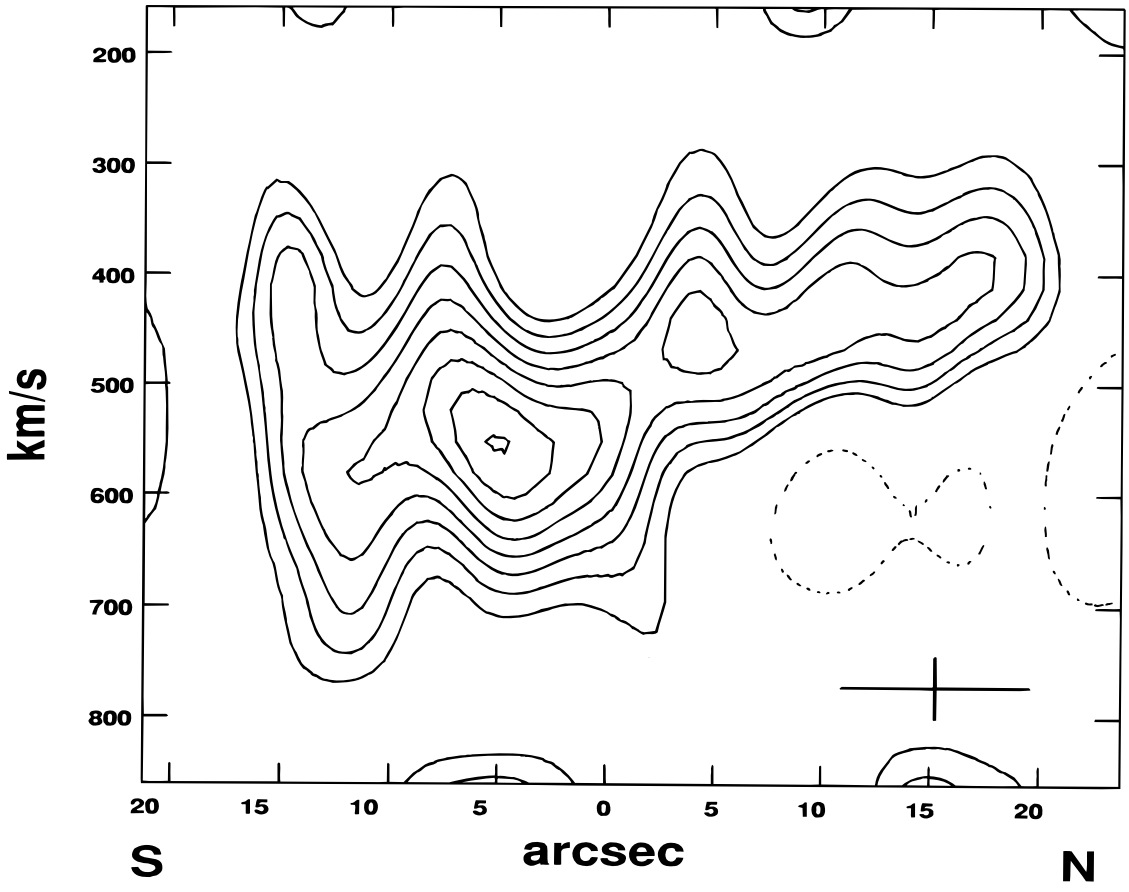

FIG. 3*b*

at a number of frequencies using the data obtained from the VLA archive. The continuum flux densities and the observing frequencies are listed in Table 3. The uncertainties in flux density (1 σ) are also given. The continuum fluxes are used below to constrain the models that explain the observed H92α line emission.

4. THE NATURE OF THE H92α LINE EMISSION FROM STARBURST GALAXIES

The typical continuum peak flux density at 8.3 GHz from the nuclear region of the galaxies observed is less than 100 mJy in a beam area of 10 arcsec.[2] The typical H92α line intensity is 1% or less of the continuum flux density. To understand the observed H92α line, we have performed a number of model calculations constrained by the available RRL and radio continuum data.

4.1. *Collective* H II *Model*

A possible model for explaining RRL emission from a starburst nuclear region is based on a collection of compact H II regions. These H II regions arise from young massive stars formed in the period of the starburst. Nonthermal

TABLE 2

RESULTS OF H92α OBSERVATIONS

Parameter	Arp 220	M83	NGC 2146	NGC 6240
Positions (1950):[a]				
R.A.	15 32 46.88	13 34 11.10	06 10 39.48	16 50 27.30
Declination	23 40 07.9	−29 36 35.7	78 22 28.89	02 28 57.5
Distance (Mpc)	74	5	13	100
Peak line flux density (mJy)[b]	0.39 ± 0.09	0.8 ± 0.15	0.36 ± 0.09	<0.3
Integrated line flux (10^{-23} W m^{-2})[b]	3.5	2.8	2.7	<2.1
Central heliocentric velocity (km s^{-1})	5560 ± 70	500 ± 30	960 ± 7	...
Line width (FWHM in km s^{-1})	320 ± 120	95 ± 30	200 ± 95	...
Beam size (FWHP in arcsec)	4.0 × 3.5	8.7 × 3.1	4.1 × 3.5	2.8 × 2.7
Position angle of the beam (deg)	56	−1	56	42
Number of beam areas in which line is observed	2	10	2.5	...
Continuum flux density (mJy)[b]	140	75	54	...
Ratio of line to continuum (%)	0.3	1	0.7	<0.4

[a] Units of right ascension are hours, minutes, and seconds; units of declination are degrees, arcminutes, and arcseconds.

[b] The quantities are determined by integrating over the region in which the line is detected. For nondetection, upper limits ($\sim 3\ \sigma$) for both peak line flux density and the integrated line flux are given assuming FWHM line width of 250 km s^{-1}.

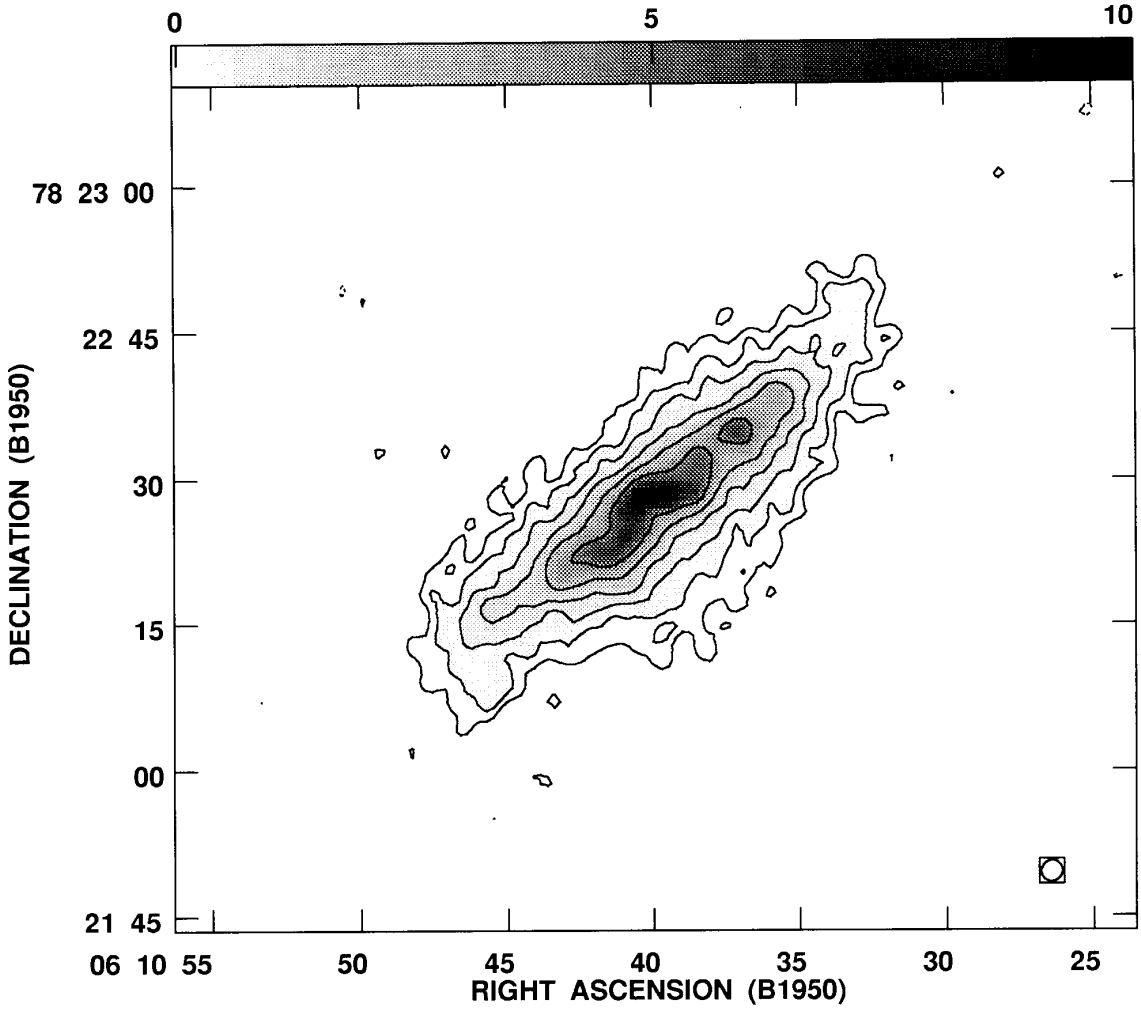

FIG. 4a

FIG. 4.—Continuum images of NGC 2146 at 8.3 GHz. (*a*) Uniform weighting, beam (FWHM) 2.″2 × 2.″1 (P.A. = −39°). Contour levels are −0.12, 0.12, 0.28, 0.44, 0.64, 0.88, 1.16, 1.48, 1.84, 2.24, 2.68, 3.16, ... mJy beam^{-1}. (*b*) natural weighting beam (FWHM) 4.″1 × 3.″9 (P.A. = −52°). Contour levels are −0.12, 0.06, 0.12, 0.24, 0.48, 0.96, 1.92, 3.84, 7.68, 15.4, 30.7, and 61.4 mJy beam^{-1}. The gray-scale representation, with a range of line flux 0–100 mJy beam^{-1} km s^{-1}, indicates the H92α line emission. (*c*) Position-velocity diagram along the major axis of the galaxy made by rotating the line images 38° clockwise. The reference position is $\alpha(1950) = 06^{h}10^{m}41^{s}.1$, $\delta(1950) = 78°22'27''$. Contours are −0.1, 0.05, 0.1, 0.15, 0.20, 0.25, and 0.30 mJy beam^{-1}. The cross indicates the resolution in both velocity and position coordinates.

radiation due to a large number of supernova remnants is responsible for most of the continuum flux density observed at 3.5 cm. It was shown in Paper I that in the cases of NGC 3628, IC 694, and NGC 1365, the models that best fit the observed RRL data require that a large number (several hundreds) of compact ($n_e > 5 \times 10^3$–5×10^4 cm^{-3}) H II regions are present within the central ~100 pc of their nuclei. The contribution from stimulated emission (ΔS_L) due to the background nonthermal source can be estimated assuming an extreme case in which the N H II regions lie in front of a uniformly distributed background emission ($S_{\rm Cbg}$),

$$\Delta S_L = N^{1/3} f_{\rm H\,II}^{2/3} \left(\frac{\Delta V_{\rm H\,II}}{\Delta V_{\rm obs}}\right) S_{\rm Cbg}\, e^{-\tau_C}(e^{-\tau_L} - 1)\,, \qquad (1)$$

assuming each H II region has the line and continuum optical depths of τ_L and τ_C and line width of $\Delta V_{\rm H\,II}$. The ratio $\Delta V_{\rm H\,II}/\Delta V_{\rm obs}$ accounts for the assumption that the observed large line width may result from the collection of H II regions being at different center velocities. We note also that equation (1) works only for small values of $N_{\rm H\,II}^{\rm los}$, the number of H II regions along the line of sight ($N_{\rm H\,II}^{\rm los} = N^{1/3} f_{\rm H\,II}^{2/3} \leq 1$), and no effects of shadowing of one H II region by another are taken into account. The shadowing effect is important only if $N_{\rm H\,II}^{\rm los} > 1$ or large and $\tau_C \geq 1$, which does not occur in any of the H II region models discussed in this paper. Due to a small volume filling factor ($f_{\rm H\,II} \sim 10^{-6}$; see Paper I) of compact H II regions in the line-emitting regions, only a small fraction of background nonthermal radiation along the line of sight interacts the H II regions. In the case of high-density compact H II regions for which both the emission measure and/or the continuum optical depths at the centimeter wavelengths are large, recombination line emission is still possible because the line optical depths become negative due to non-LTE effects. However, since the background continuum emission intercepted by an H II region is small, the line emission generated within the H II region (including the stimulated emission due to its own continuum emission) far exceeds the external stimulated emission. For example, in the case of Arp 220, assuming $T_e = 5 \times 10^3$ K, $n_e = 10^4$ cm^{-3}, $\Delta V_{\rm H\,II} = 20$ km s^{-1}, and size of 2.5 pc, the continuum optical depth at 8.3 GHz $\tau_C = 2.4$ and the line optical depth $\tau_L = -4$. About 100 such H II regions are required to account for the observed

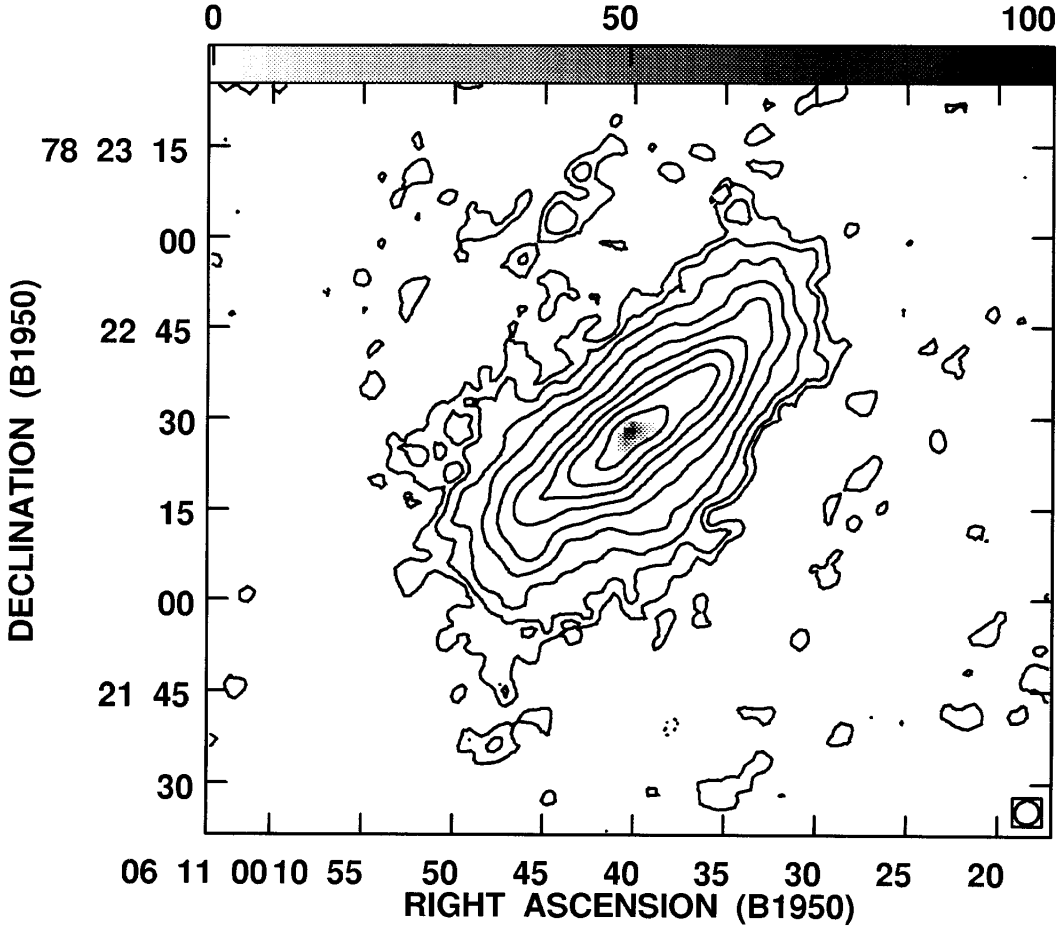
0
50
100
78 23 15
00
22 45
30
15
00
21 45
30
DECLINATION (B1950)
06 11 00
10 55
50
45
40
35
30
25
20
RIGHT ASCENSION (B1950)

FIG. 4*b*

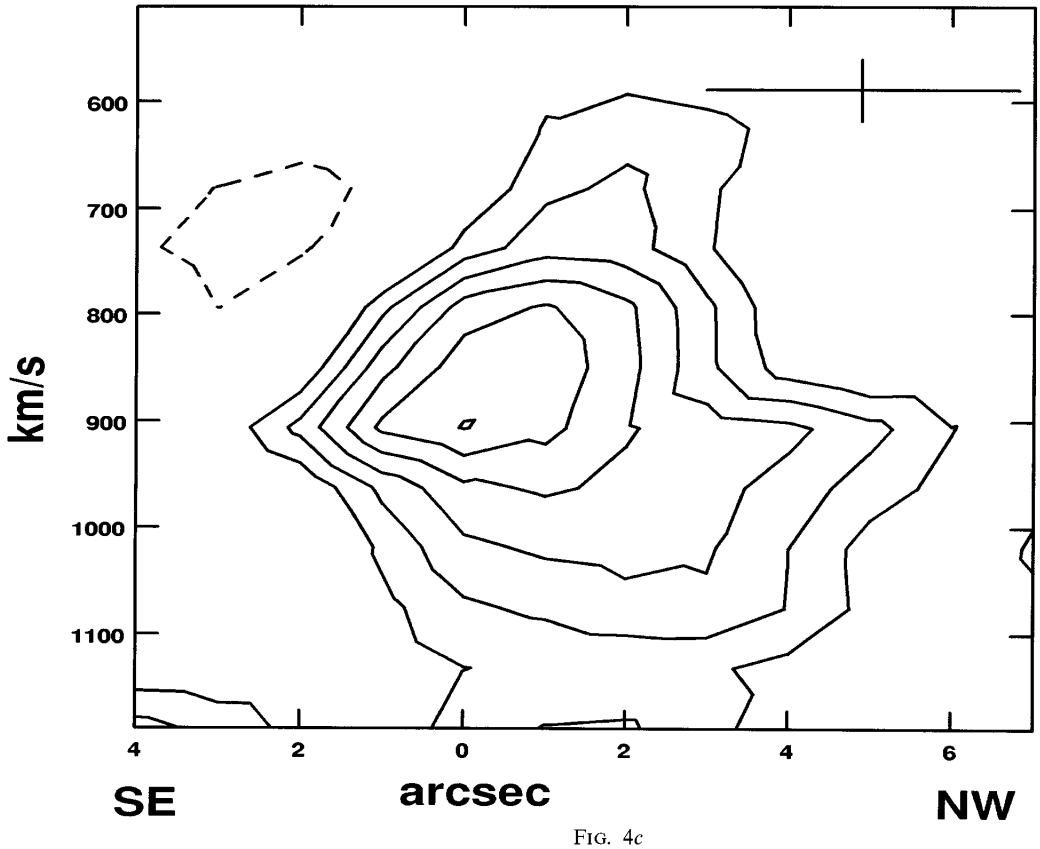
600
700
800
900
1000
1100
km/s
4
2
0
2
4
6
SE
arcsec
NW

FIG. 4*c*

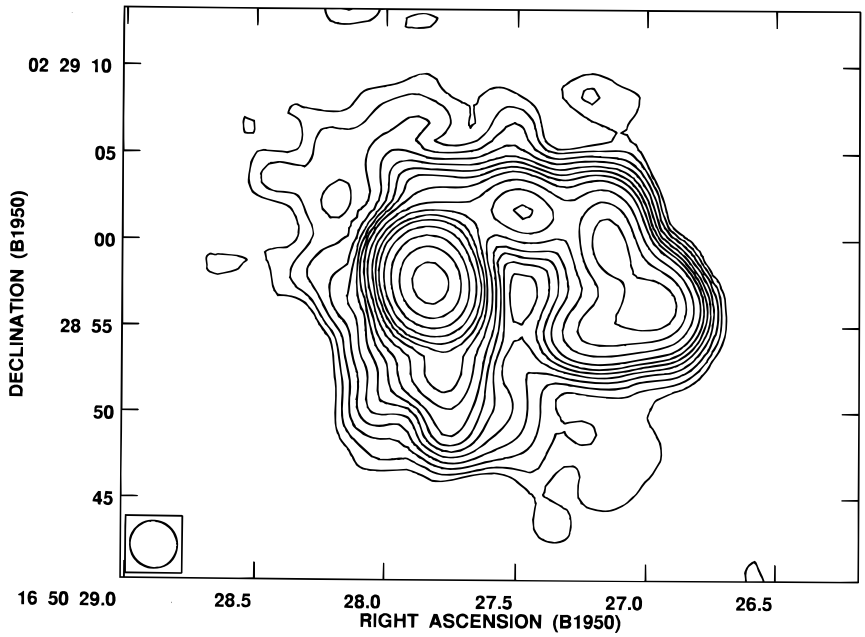

FIG. 5.—Continuum image of NGC 6240 observed at 8.1 GHz. Contours are −0.08, 0.06, 0.10, 0.16, 0.24, 0.34, 0.46, 0.60, 0.80, 1.2, 1.8, 2.6, ... mJy beam^{-1} (FWHM beam size 2.″9 × 2.″8, P.A. = 41°).

line emission. For these H II regions, the contribution from external stimulated emission calculated using the above equation is less than 1% of the internal line emission. Note that in this particular example, the total optical depth (i.e., $\tau_C + \tau_L$) is negative, and still the contribution from external stimulated emission is small compared to the internal emission. In fact, if the total optical depth is decreased further to even larger negative values, the fractional contribution from external stimulated emission becomes even smaller because the internal emission increases at a faster rate. Thus, in all models that consist of a collection of compact high-density H II regions, stimulated emission due to the nonthermal background is negligible.

On the other hand, for low-density models (e.g., $n_e = 50$ cm^{-3}, $T_e = 5000$ K), the contribution from external stimulated emission is significant compared to the internal emission. In a model constructed for Arp 220 with the above parameters, about 3×10^7 such H II regions are required to account for the observed line emission, and roughly equal contribution to the line comes from external stimulated emission and internal emission from each H II region. It was shown in Paper I that for the galaxies NGC 3628, IC 694, and NGC 1365, such low-density models in general fail to satisfy other constraints such as the observed continuum spectrum.

TABLE 3

CONTINUUM FLUX DENSITY IN THE H92α LINE EMISSION REGION

Flux Density (MJy)	Observing Frequency (GHz)
Arp 220	
90 ± 6	22.5
104 ± 2	15
145 ± 1	8.4
210 ± 2	4.7
332 ± 4	1.6
296 ± 5	1.4
M83	
50 ± 4	15
75 ± 1	8.3
NGC 2146	
37 ± 2	15
54 ± 1	8.3
84 ± 5	5
153 ± 7	1.5

Utilizing the collective compact H II region model discussed in Paper I, we have calculated the RRL flux densities and the continuum flux densities as a function of frequency for several combinations of T_e, n_e, and the size of the H II region. The models are then constrained by the observed line and continuum strengths and some physical and geometrical considerations, as discussed in Paper I. At centimeter wavelengths, the contribution from the dust blackbody radiation to the background continuum radiation is negligible. No thermal dust emission has been considered in the following calculations. The model parameters are summarized in Tables 4, 5, and 6. We defined the non-LTE factor as the ratio of the line emission intensity corrected for the non-LTE effect to the LTE value ($S_{\mathrm{Hn}\alpha}/S^*_{\mathrm{Hn}\alpha}$) assuming no contributions from external stimulated emission. The values of fractional stimulated emission, namely, the percentage of the stimulated line intensity due to the background nonthermal radiation in the total line intensity, are also given.

4.1.1. *Arp 220*

For Arp 220, the input constraints are a single line (H92α) measurement and a number of continuum observations. The model results are plotted in Figure 6, and the model parameters are summarized in Table 4. For $T_e = 5 \times 10^3$–1×10^4 K, densities in the range 50–10^4 cm^{-3} are acceptable. The mean H II region size of 2.5 pc is assumed.

In general, for higher density models ($n_e \geq 1 \times 10^4$ cm^{-3}), the number of H II regions required to explain the

TABLE 4

MODEL RESULTS FOR COLLECTION OF H II REGIONS: ARP 220

PARAMETER	MODEL			
	A	B	C	D
T_e (K)	5×10^3	5×10^3	5×10^3	1×10^4
n_e (cm^{-3})	50	5×10^2	1×10^4	1×10^4
Size (pc)	2.5	2.5	2.5	2.5
$N_{\rm H\,II}$	3×10^7	3×10^5	110.	640
$N_{\rm H\,II}^{\rm los}$	56	0.5	2×10^{-4}	1×10^{-3}
Filling factor	7×10^{-2}	7×10^{-4}	3×10^{-7}	1×10^{-6}
τ_C (at 8.3 GHz)	6×10^{-5}	6×10^{-3}	2.4	0.95
τ_L (at 8.3 GHz)	-8×10^{-4}	-6×10^{-2}	-4	-0.9
Non-LTE factor (H92α)	0.77	1.1	170	17
Stimulated emission (% H92α)	51	36	1	1
$S_{\rm th}$ (at 5 GHz) (mJy)	19	18	0.4	4.1
$S_{\rm nth}$ (at 5 GHz) (mJy)	165	166	183	179
Spectral index ($\alpha_{\rm nth}$)	-0.58	-0.57	-0.53	-0.58
Total ionized mass ($M_\odot$)	3×10^8	3×10^7	2×10^5	1×10^6
$N_{\rm Lyc}$($\times 10^{54}$ s^{-1})	8.9	8.3	1.2	4.0
Number of O5 stars ($\times 10^5$)	1.9	1.8	0.3	0.9

line emission increases with increasing temperature. Both spontaneous and internal stimulated emission are dominant in the H92α line in the high-density H II region model. The high-density models predict that the hydrogen radio recombination lines for $\Delta n = 1$ or the H$n\alpha$ lines reach a maximum in intensity around 22 GHz.

The lower density models are dominated by stimulated emission due to the background nonthermal emission. These lower density models require a large number of H II regions ($N_{\rm H\,II}$) and a large filling factor in comparison with the high-density models. In addition, the low-density models require a larger amount of ionized gas (see Table 4). To maintain the ionization, a larger ionizing photon rate or a larger number of OB-type stars is needed. For $T_e = 5 \times 10^3$ K and $n_e = 50$ cm^{-3}, the predicted $N_{\rm Lyc} = 8.9 \times 10^{54}$ s^{-1}, which can be produced by 2×10^5 O5 stars. When n_e is increased to 10^4 cm^{-3}, the predicted $N_{\rm Lyc}$ is 1.2×10^{54} s^{-1}, which corresponds to 3×10^4 O5 stars. It is not surprising that Arp 220 has the largest amount of ionized gas and Lyman-continuum flux among the three detected sources.

The lower density models predict high RRL flux densities at lower frequencies. For example, the expected RRL flux density at 20 cm is about 2–3 mJy for $N_e \sim 50$ cm^{-3}. Lower frequency line observations will be decisive in selecting the appropriate model.

4.1.2. *M83*

In order to fit the observed data, about 100–300 H II regions with sizes 0.5–5 pc with $n_e = 5 \times 10^2$–5×10^4 cm^{-3} and $T_e = 0.5$–1×10^4 K are required for M83. A number of models (summarized in Table 5) have been calculated, constrained by the available data. The line flux densities as a function of frequency as well as the continuum spectra for these models are plotted in Figure 7. The high-density model (5×10^4 cm^{-3}) is distinct from the rest of the models.

TABLE 5

MODEL RESULTS FOR COLLECTION OF H II REGIONS: M83

PARAMETER	MODEL				
	A	B	C	D	E
T_e (K)	5×10^3	5×10^3	5×10^3	7.5×10^3	7.5×10^3
n_e (cm^{-3})	5×10^2	1×10^3	1×10^4	1×10^4	5×10^4
Size (pc)	5	5	0.5	0.5	0.5
$N_{\rm H\,II}$	330	52	370	830	130
$N_{\rm H\,II}^{\rm los}$ (10^{-3})	29	4.6	0.3	0.7	0.1
Filling factor (10^{-6})	270	43	0.3	0.7	0.1
τ_C (at 8.3 GHz)	0.01	0.05	0.47	0.28	7.0
τ_L (at 8.3 GHz)	-0.11	-0.33	-0.77	-0.34	-1.7
Non-LTE factor (H92α)	1.3	2.1	5.4	3.5	1200
Stimulated emission (% H92α)	2.8	1.4	0.2	0.2	<0.001
$S_{\rm th}$ (at 5 GHz) (mJy)	19	11	4.7	12	3.3
$S_{\rm nth}$ (at 5 GHz) (mJy)	90	96	102	97	153
Spectral index ($\alpha_{\rm nth}$)	-0.91	-0.81	-0.79	-0.91	-1.7
Total ionized mass ($M_\odot$)	3×10^5	8×10^4	6×10^3	1×10^4	1×10^4
$N_{\rm Lyc}$(10^{52} s^{-1})	7.2	4.6	3.3	5.2	20
Number of O5 stars (10^2)	15	9.8	7.0	11	44

TABLE 6

MODEL RESULTS FOR COLLECTION OF H II REGIONS: NGC 2146

PARAMETER	MODEL				
	A	B	C	D	E
T_e (K)	5×10^3	5×10^3	7.5×10^3	7.5×10^3	5×10^3
n_e (cm^{-3})	5×10^3	1×10^4	5×10^4	1×10^4	1×10^5
Size (pc)	1	1	0.5	1	0.2
$N_{\rm H\,II}$	637	97	450	230	135
$N_{\rm H\,II}^{\rm los}$ (10^{-3})	4.6	0.7	0.8	1.6	0.04
Filling factor (10^{-6})	12	1.9	1.1	4.5	0.02
τ_C (at 8.3 GHz)	0.24	0.95	7.0	0.65	20
τ_L (at 8.3 GHz)	−0.65	−1.5	−1.7	−0.68	3.6
Non-LTE factor (H92α)	4	15	1180	7	1
Non-LTE factor (H53α)	1	1.8	8.9	1.3	130
Stimulated emission (% H92α)	2	0.6	0.003	0.6	−0.8
$S_{\rm th}$ (at 5 GHz) (mJy)	5.9	1.7	3.1	5.2	0.09
$S_{\rm nth}$ (at 5 GHz) (mJy)	69	74	82	71	...
Spectral index ($\alpha_{\rm nth}$)	−0.76	−0.72	−1.2	−0.82	...
Total ionized mass ($M_\odot$)	4×10^4	1×10^4	4×10^4	3×10^4	1×10^3
$N_{\rm Lyc}$ (10^{53} s^{-1})	1.1	0.68	7.2	1.2	0.7
Number of O5 stars (10^3)	2.4	1.5	1.5	2.5	1.7

The upper limit of the H53α observation implies that only models with $n_e < 5 \times 10^4$ cm^{-3} are compatible with the data. The rate of ionizing photons ($N_{\rm Lyc}$) is required in these models is in the range 3×10^{52}–2×10^{53} s^{-1}, consistent with that derived from infrared hydrogen recombination line observations (Turner et al. 1987). Roughly 10^3 O5 stars are required if the ionization is due to young stars. Further observations in both continuum and RRLs are necessary to determine the model parameters uniquely.

4.1.3. *NGC 2146*

Based on the detection of the H53α line (40″ beam), Puxley et al. (1991) carried out model calculations. Within a reasonable temperature range (0.5–1×10^4 K), they found that a collective compact H II region model with $n_e \geq 10^4$ cm^{-3} can satisfy the restrictions imposed by the total H53α line flux and the continuum flux density at 5 GHz. The VLA observations of H92α show that the RRL emission is concentrated in the nuclear region with an angular size of $\sim 10''$ (600 pc). From the data obtained from the VLA archives, we have also determined continuum flux densities corresponding to the line emission region at frequencies in the range 1.5–15 GHz (see Table 3). The available data from both line and continuum measurements provide critical restrictions on the model calculations. To fit both H92α and H53α line flux densities, the electron density needs to be greater than

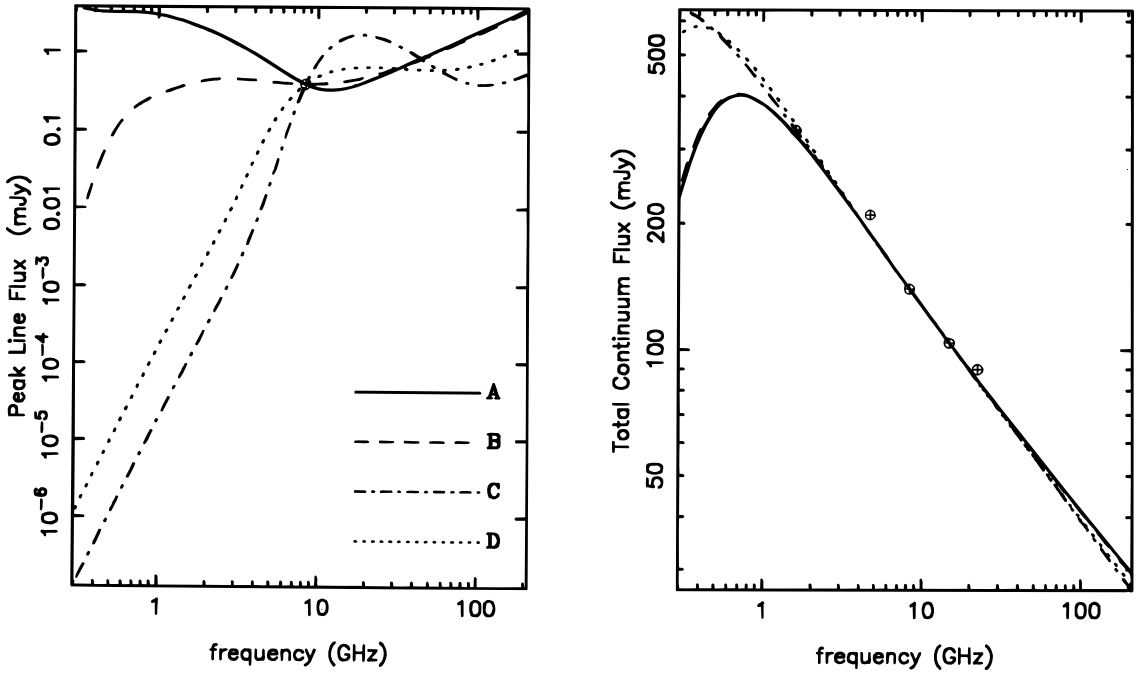

FIG. 6.—Arp 220. *Left*: Peak H$n\alpha$ line flux density as a function of frequency for models of a collection of H II regions. *Right*: The predicted continuum spectra for a collection of H II regions. These models fit the observed RRL and radio continuum data (indicated as circled plus signs) in Arp 220. The model parameters are summarized in Table 4.

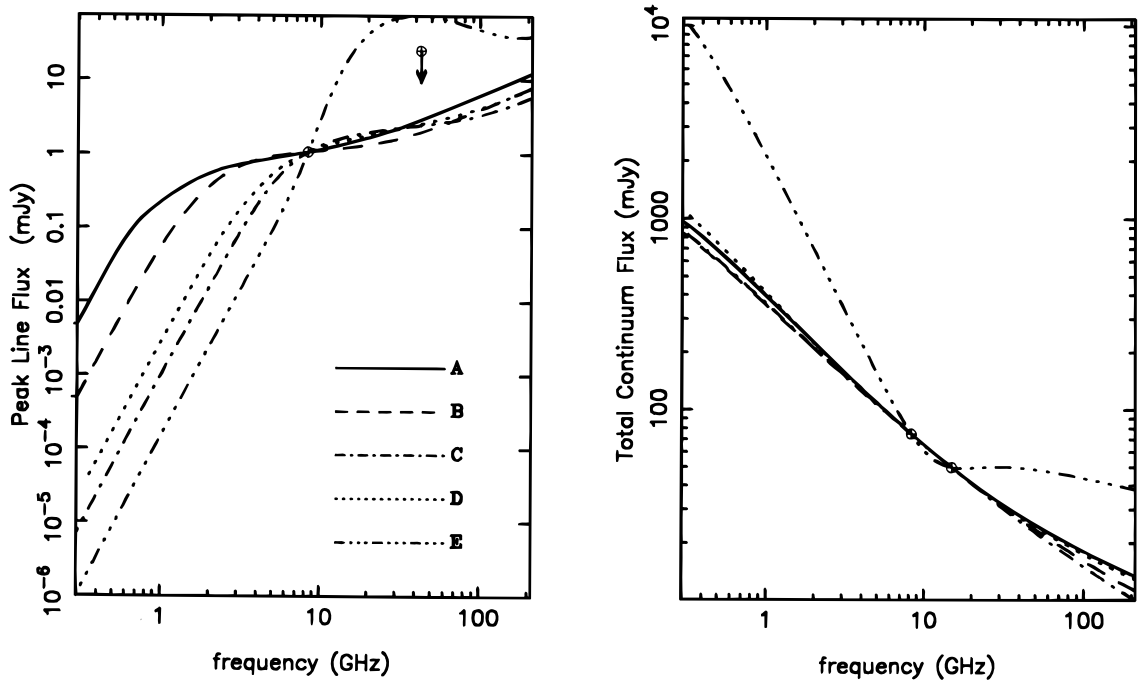

FIG. 7.—M83. *Left*: Peak H$n\alpha$ line flux density as a function of frequency for models of a collection of H II regions. *Right*: The predicted continuum spectra for a collection of H II regions. These models fit the observed RRL and radio continuum data (indicated as circled plus signs) in M83. The model parameters are summarized in Table 5.

5×10^4 cm^{-3}. However, such models provide a poor fit to the continuum spectrum (see model C in Table 6 and Fig. 8*a*). The high-density model produces too much continuum at shorter wavelengths due to free-free emission, possibly in conflict with the 2 cm continuum (Fig. 8*a*). More measurements at centimeter to millimeter wavelengths are required to determine if the high-density model can be excluded.

Alternatively, using the VLA data only, we obtain a number of models (A, B, and D in Fig. 8*a*) that fit both the continuum spectrum and the H92α line flux density but not the H53α data. It is difficult to reconcile a model with single density with the observations of both H92α and H53α line data as well as the radio continuum. On the other hand, we consider also a model composed of compact H II regions with a very high density. This model can produce desirable line flux for the H53α transition but little free-free continuum because of a large non-LTE factor at millimeter wavelengths and a large continuum optical depth at centimeter wavelengths (see model E in Table 6). Each of the high-density compact H II regions ($n_e = 1 \times 10^5$ cm^{-3}, $T_e = 5 \times 10^3$ K, and size of 0.2 pc) has a large negative value in total optical depth ($\tau_L + \tau_C \sim -5$ at 43 GHz). The non-LTE factor for the H53α line is 130. Thus, a model combining one of the lower density components (e.g., model A) with the high-density component (model E) does fit both the line and continuum data (see Fig. 8*b*). The resultant model shows that the line intensity is peaked around 50 GHz due to the large non-LTE factor. The lines at millimeter wavelengths are highly stimulated by the free-free emission from the high-density compact H II regions themselves.

In the above models, the geometrical size of the H II region is a chosen parameter ranging from 0.01 to 10 pc. Some of the models with certain sizes do not pass all the constraints imposed by the observations. For example, if the size is too small, the model will produce too much thermal continuum emission. The large size H II region model may require too few H II, regions and each of such H II regions produces a peak line intensity that is much higher than that observed in the integrated profile (see Paper I). We presented some of the models that pass the constraints. We note also that different sizes do affect the output parameters such as the total ionized mass (and/or the volume filling factor) and the fraction of stimulated emission due to the nonthermal background radiation. For high-density cases, an increase in H II region size results in increases of optical depths in both continuum and line and therefore an enhancement in non-LTE factor. Consequently, the total H II mass or the volume filling factor is reduced in larger size H II region models, and the stimulated emission due to the nonthermal background emission is less important in the models of H II regions with a large geometrical size.

For low-density cases, because the H II regions are optically thin, the filling factor and/or the total H II mass remain nearly the same as the geometrical size changes.

4.2. *Slab Model*

Alternative to the collective H II region model, a uniform slab of ionized gas in front of the background continuum source can also be considered. As discussed in Paper I, the line flux density is then composed of two components: (1) the internal line emission of the slab including the spontaneous emission and the stimulated emission due to the free-free continuum arising from the ionized gas (optically thin gas),

$$S_L^{(1)} \approx \frac{2kv^2 b_n}{c^2} \tau_L^* \Omega_L T_e \left(1 - \frac{\beta_n \tau_C}{2}\right), \quad (2)$$

and (2) the external stimulated emission due to the background continuum,

$$S_L^{(2)} \approx \tau_L S_{\rm Cbg}, \quad (3)$$

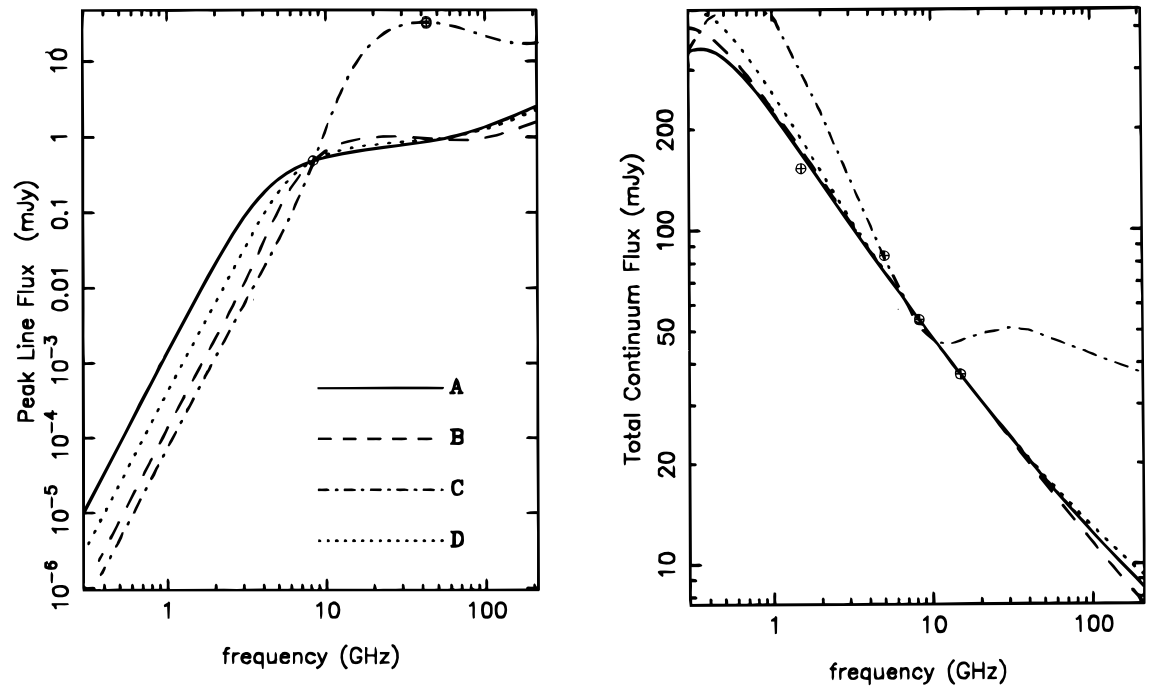

FIG. 8*a*

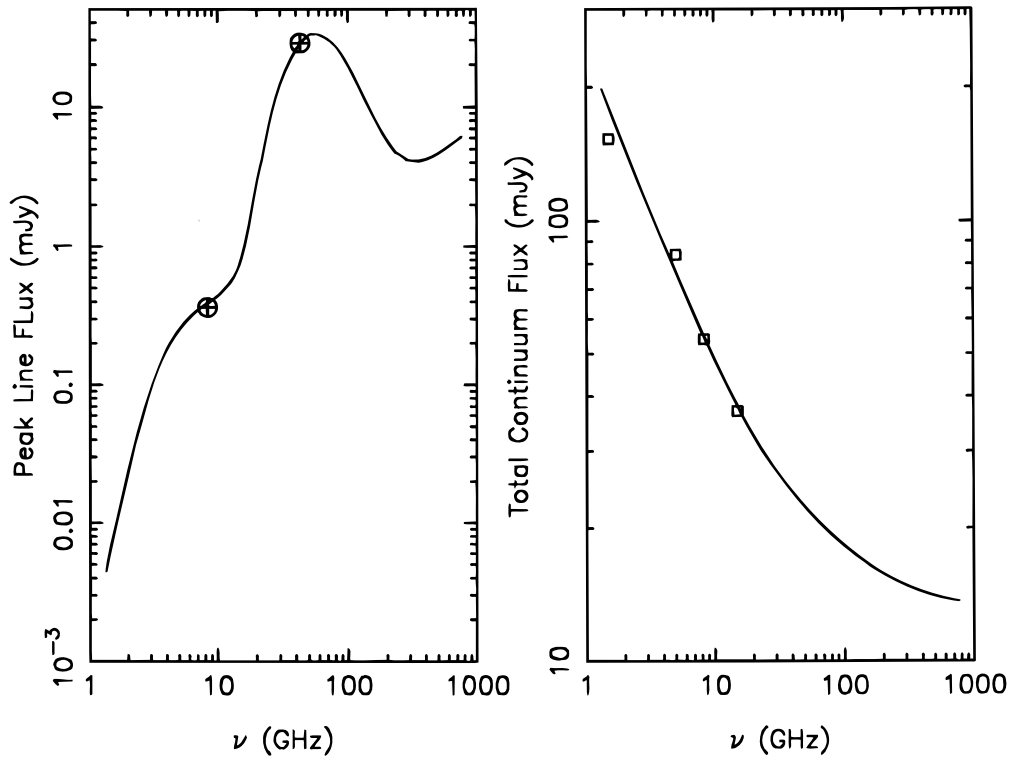

FIG. 8*b*

FIG. 8.—(*a*) NGC 2146. *Left*: Peak H$n\alpha$ line flux density as a function of frequency for models of a collection of H II regions. *Right*: The predicted continuum spectra for a collection of H II regions. These models are compared to the observed RRL and radio continuum data (indicated as circled plus signs) in NGC 2146. The model parameters are summarized in Table 6. (*b*) A model combining the very high density compact H II region component (case E) with the lower density H II region component (case A) fits both the line and continuum data of NGC 2146.

where c, k, and T_e are the speed of light, Boltzmann's constant, and electron temperature; b_n and β_n are the LTE departure coefficients; ν and Ω_L are the observing frequency and the solid angle covering the line emission region; and τ_L^* and τ_C are the LTE line and continuum optical depths, respectively. The line optical depth is given by $\tau_L = b_n \beta_n \tau_L^*$. The volume filling factor in the slab model is unity. The background continuum emission, $S_{\rm Cbg}$, is dominated by nonthermal synchrotron emission ($S_{\rm nth} \propto \nu^{\alpha_{\rm nth}}$) at centimeter and longer wavelengths or by thermal dust

TABLE 7

MODEL PARAMETERS FOR SLAB UNIFORM IONIZED GAS

PARAMETER	ARP 220		M83	
	Model A	Model B	Model A	Model B
T_e (K)	5×10^3	1×10^4	5×10^3	5×10^3
n_e (cm^{-3})	1×10^4	100	5×10^3	500
Path length (pc)	0.005	85	0.0015	0.15
EM (pc cm^{-6})	5×10^5	8×10^5	3.8×10^4	3.7×10^4
Spectral index:				
$\alpha_{\rm nth}$	-0.7	-0.75	-0.39	-0.39
$\alpha_{\rm dust}$	3.3	3.3	...	...
$S_L^{(1)}(H92\alpha)$ (mJy)	0.3	0.08	0.78	0.75
$S_L^{(2)}$ (H92α) (mJy)	0.09	0.31	0.02	0.05
Stimulated emission (%)	22	81	2.5	6.3
Total ionized mass ($M_\odot$)	3.4×10^7	5.8×10^8	5.2×10^4	5.3×10^5
$N_{\rm Lyc}$($\times 10^{54}$ s^{-1})	27	29	0.14	0.14
Number of O5 stars ($\times 10^3$)	600	700	3	3

(blackbody) at millimeter and shorter wavelengths. In the optically thin blackbody case, $S_{\rm dust} \propto \nu^{\alpha_{\rm dust}}$ and $\alpha_{\rm dust} = \beta + 2$, where β is the power-law index of the dust emissivity ($\epsilon \propto \nu^\beta$) and the Rayleigh-Jeans law applies at the radio wavelengths. Thus, the total continuum flux density arises from the three components, namely, the nonthermal synchrotron, free-free emission ($S_{\rm ff}$), and thermal dust emission:

$$S_{\rm Cbg} = S_{\rm nth} + S_{\rm ff} + S_{\rm dust} . \quad (4)$$

In the case of Arp 220, there are several uniform slab models with $T_e \geq 5000$ K that fit the data. We have considered two cases in the following: model A, with a high density, lower temperature, and thin slab ($n_e = 1 \times 10^4$ cm^{-3}, $T_e = 5 \times 10^3$ K, path length of $L_{\rm path} = 0.005$ pc), and model *B*, with a low density, higher temperature, and thick slab ($n_e = 1 \times 10^2$ cm^{-3}, $T_e = 1 \times 10^4$ K, $L_{\rm path} = 85$ pc). The model parameters are summarized in Table 7. Figure 9*a* shows the H$n\alpha$ line flux density as a function of frequency (*dashed curve*) and continuum spectrum calculated (*solid curve*) from the two slab models (A and B). Both models predict that the line is primarily spontaneous emission at high frequencies. The contribution from both the external and internal stimulated emission can be ignored at high frequencies (or millimeter wavelengths) in the uniform slab model because of small optical depths in both the line and continuum.

Figure 9*a* also shows the ratio of the line flux density stimulated by the background radiation to the total line flux density $[S_L^{(2)}/(S_L^{(1)} + S_L^{(2)})]$ (*dot-dashed curve*). The external stimulated emission appears to be dominant at lower frequencies in both models A and B. The low-density model predicts that the line flux density increases at lower frequencies and is peaked around 1 GHz. In the high-density model, the line flux density decreases as the frequency decreases. The two models are distinguishable at the low frequencies. Further observations of H$n\alpha$ lines will be crucial in distinguishing between these high- and low-density models. The VLA at 1.5 GHz appears to be the best instrument for this task. Finally, we note that the slab models require an ionizing photon rate that is an order of magnitude higher than the collection of H II region models.

Some slab models with $T_e = 5000$ K can fit the M83 data. Figure 9*b* shows a high-density, thin slab (model A) versus a lower density, relatively thick slab (model B). Both models suggest that the line emission at 8.3 GHz is primarily internal. The contribution from the external stimulated emission to the H92α line is less than 10%. However, the low-density model predicts that the external stimulated emission is dominant at 1 GHz. In comparison with the H II region models, the slabs require a large H II mass and more O5 stars for ionization.

There are no uniform slab models with $T_e \geq 5 \times 10^3$ K that fit the data observed in NGC 2146.

5. DISCUSSION

5.1. *Comparison with Brα*

Hydrogen Brackett line observations provide an independent probe of the heavily obscured nuclear region in starburst galaxies. The Brα line has been detected from several nearby starburst galaxies (Rieke, Liebofsky, & Walker 1988, Depoy, Becklin, & Geballe 1987; Kawara, Nishida, & Phillips 1989; Ho, Beck, & Turner 1990). Combining previously published data with our new observations, we can construct a sample of 13 starburst galaxies that have been searched for RRLs with the VLA. Most of these galaxies have been detected in the Brα line. Nine out of the 13 galaxies have been detected at H92α. In order to investigate the probability of correlation between H92α and Brα lines, we plot the H92α line luminosity versus the Brα line luminosity with no extinction corrections (Fig. 10). There has been debate over whether correlations are measured more accurately by comparing the observed flux densities or intrinsic luminosities. Various authors suggest that plotting the flux versus flux will alleviate selection effects present in the luminosity diagram. Though the distance dependence will be removed, intrinsic correlations between the two luminosities can be lost in the flux-flux diagram (Feigelson & Berg 1983). The authors also show that luminosity-luminosity diagrams provide a well-defined way to determine whether or not emission at the two frequencies is intrinsically related. Flux-flux diagrams do not provide such a definitive test.

Since our data set involves upper limits in both variables, we employed a statistical technique called survival analysis to examine the relationship between the H92α and Brα luminosities. The generalized Kendall's rank correlation (GKR) test is one of the powerful methods that is effective to test doubly limited data (Isobe, Feigelson, & Nelson

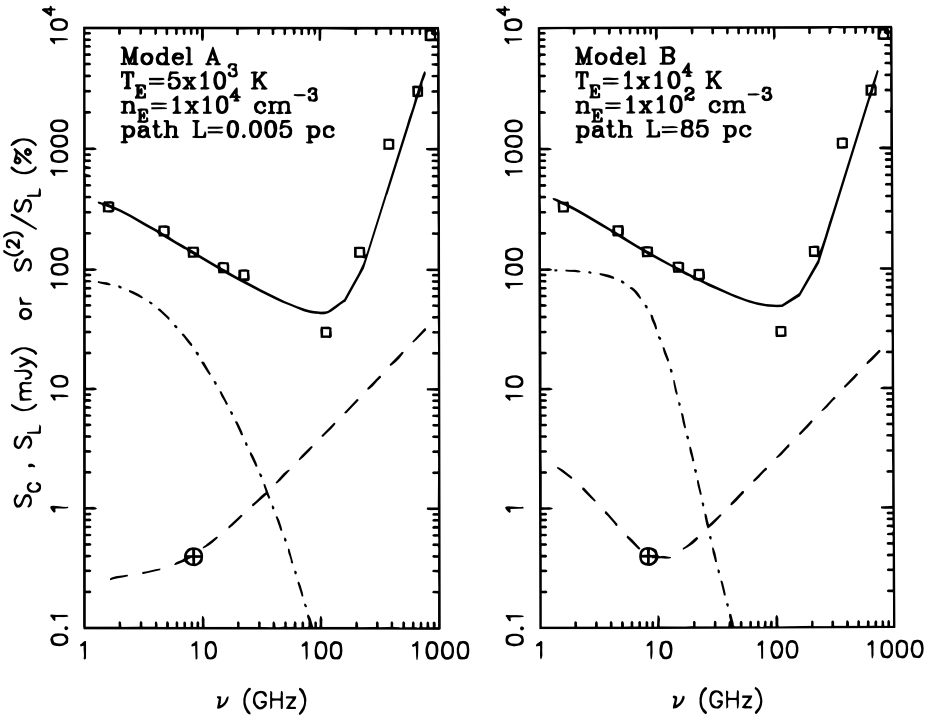

FIG. 9*a*

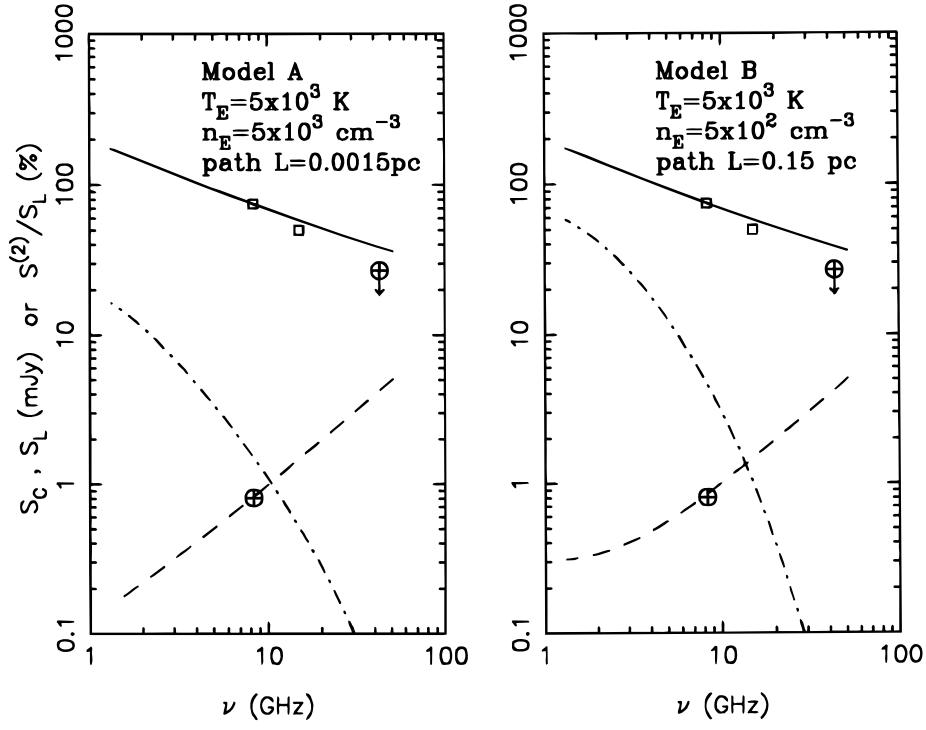

FIG. 9*b*

FIG. 9.—(*a*) Arp 220. Peak H$n\alpha$ line flux density as a function of frequency and continuum spectrum calculated from two slab models (A and B) of uniform ionized gas for Arp 220 described in the text and Table 7. The continuum spectrum is based on the data (*squares*) from this paper, Scoville et al. (1991), Eales, Wynn-Williams, & Duncan (1989), and Woody et al. (1989). The solid curve is the continuum spectrum calculated from the slab models. The dashed curve is the line intensity of H$n\alpha$ fitted to the observed H92α data (*circled plus signs*). The dash-dotted curve indicates the fraction of the stimulated line due to background continuum in H$n\alpha$ lines as function of frequency. (*b*) Uniform slab models of higher density (*left*) and lower density (*right*) fit the line (*circled plus signs*) and continuum (*squares*) data of M83. The solid curve is the continuum spectrum calculated from the slab models. No dust component is considered in the calculations. The dashed curve is the line intensity of H$n\alpha$. The dash-dotted curve indicates the fraction of the stimulated line due to background continuum in H$n\alpha$ lines as function of frequency.

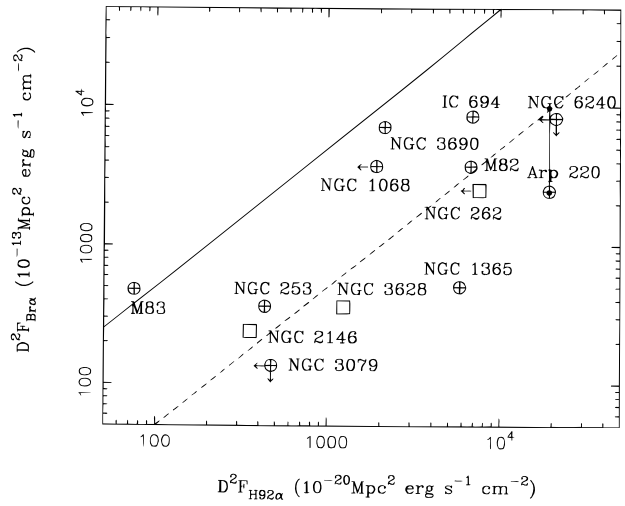

FIG. 10.—The H92α line luminosity vs. Brα line luminosity. The solid diagonal line shows the LTE relation between H92α and Brα. The dashed curve indicates the H92α- Brα line relation with correction for the non-LTE effects assuming that the non-LTE factor is 10. The vertical line is the Brα line luminosity corrected for infrared extinction ($A_{4\,\mu m} = 1.5$ mag). Most of the H92α data are from Paper I and this paper. The data for NGC 253, M82, and NGC 3690 are from Anantharamaiah & Goss (1990), Seaquist et al. (1994), and Zhao et al. (1996), respectively. The Brα data without correction for extinction (Ho et al. 1990; Depoy et al. 1986, 1987; Kawara et al. 1989) are indicated by circled plus signs. For NGC 262, NGC 2146, and NGC 3628, the Brα data are derived from Paβ, Brγ, and Hα observations (Ruiz, Rieke, & Schmidt 1994; Hutchings et al. 1990; Fabbiano, Heckman, & Keel 1990), respectively.

1986). A significant correlation between the $D^2F_{H92\alpha}$ and $D^2F_{Br\alpha}$ exists for the starburst galaxies. The GKR test indicates that the probability of correlation is 96%.

The intrinsic H92α line flux ($F^*_{H92\alpha}$) is, under LTE conditions and case B (Osterbrock 1989), linearly proportional to the intrinsic Brα line flux ($F_{Br\alpha}$) for optically thin gas, $T_e = 10^4$ K and $n_e = 10^4$ cm^{-3}:

$$F^*_{H92\alpha} \approx 2 \times 10^{-8}\ \text{ergs}^{-1}\ \text{cm}^{-2}\left(\frac{F_{Br\alpha}}{\text{ergs}^{-1}\ \text{cm}^{-2}}\right). \quad (5)$$

The ratio $F^*_{H92\alpha}/F_{Br\alpha}$ depends weakly on the electron temperature and density. The uncertainty in the H92α line flux is less than 20% with an uncertainty of about a factor of 2 in both the electron temperature and electron density. The solid diagonal curve in Figure 10 reflects the LTE relation between $D^2F_{H92\alpha}$ and $D^2F_{Br\alpha}$ for an electron temperature of 10^4 K and a density of 10^4 cm^{-3}. However, all the galaxies except M83 show an excess of H92α line intensities as compared to the LTE predictions. There are two possibilities for causing this deviation from the predicted LTE curve: First, the extinction at $\lambda = 4.05$ μm is not negligible. The typical $A_{4\,\mu m}$ lies in the range of <1 mag for those nuclear sources based on the estimate from the ratio of Brα to Brγ (Ho et al. 1990). The extinction to the nucleus of Arp 220 may be even larger. As suggested by the silicate absorption depth, the visual extinction is $A_v = 50$ mag (Becklin & Wynn-Williams 1987) or $A_{4\,\mu m} = 1.5$ mag assuming $A_{4\,\mu m} = 0.03A_v$ (Becklin et al. 1978). Thus, the intrinsic $F_{Br\alpha}$ could be a factor of 4 greater than the observed value. The correction for the infrared extinction will increase $F_{Br\alpha}$ but is still not sufficient to explain the excess $F_{H92\alpha}$ intensity.

Alternatively, the non-LTE effects on the level populations at large quantum numbers could cause an enhancement in the H92α line. Based on the H II region model calculations, we find that for compact high-density H II regions the non-LTE factor is large (see Tables 4, 5, and 6). For example, model C for Arp 220 ($T_e = 5 \times 10^3$ K, $n_e = 10^4$ cm^{-3}, size of 2.5 pc) predicts the non-LTE factor of 170. Most of the models with the density and temperature in the ranges of $n_e = 5 \times 10^3$–5×10^4 cm^{-3} and $T_e = 5 \times 10^3$–5×10^4 K show that the value of the non-LTE factor is around 10 (dashed line in Figure 10).

However, for the low-density models (such as models A and B for Arp 220), the non-LTE factor is small (even less than 1 in the model A), but the contribution from external stimulated emission is large. Either of these effects will alter the relation.

5.2. *Comparison with Dense Molecular Gas*

HCN and HCO^+ are among the most abundant molecules after CO. These high dipole moment molecules require density $n(H_2) > 10^4$ cm^{-3} for collisional excitation and therefore trace the dense cores within molecular clouds that may be related directly to star formation. This molecular hydrogen density appears to be similar to the electron density required by the RRL observations. Of particular interest is the global spatial correlation between the dense molecular cores and compact H II regions in these starburst galaxies. The line emission of HCN and HCO^+ has been surveyed with the IRAM 30 m telescope for nearby starbursts (Nguyen-Q-Rieu et al. 1992) and for ultraluminous IR galaxies (Solomon, Downes, & Radford 1992). We find that the H92α line luminosity correlates strongly with the line luminosity of HCN or HCO^+ (Fig. 11). The GKR test shows that the correlation probability is 99%. The tight correlation between H92α and HCN or HCO^+ indicates that the ionized gas appears to be associated with the dense molecular cloud, suggesting the presence of massive star formation within the dense molecular cores in these starburst nuclei.

This correlation could also imply that the average electron density of the H II regions emitting RRLs could be as high as the dense molecular medium ($n_e > 10^4$ cm^{-3}). For

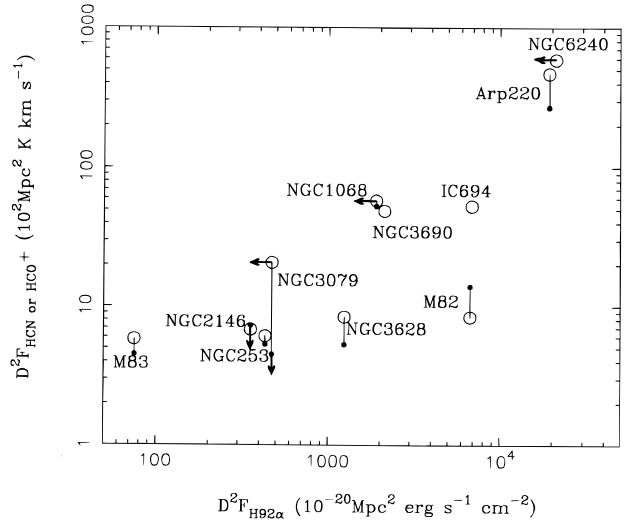

FIG. 11.—H92α line luminosities are plotted vs. dense molecular gas as traced by HCN (*circles*) and HCO^+ (*dots*). The H92α line data are discussed in Fig. 10. The HCN(1–0) and HCO^+(1–0) data were observed with the IRAM 30 m at 3 mm (Nguyen-Q-Rieu et al. 1992; Solomon et al. 1992).

higher densities, the non-LTE effects become more important at high frequencies (or low principal quantum number); for example, for $n_e = 3 \times 10^5$ cm^{-3} and $T_e = 10^4$ K, $\tau_l \approx -14\tau_l^*$ for $n = 30$ at 232 GHz, where τ_l^* is the LTE line optical depth ($\tau_l^* = 0.16$ for an H II region of 0.2 pc in size). Thus, searching for RRLs from the high-density medium in starburst galaxies at shorter millimeter or submillimeter wavelengths is promising.

6. CONCLUSION

We have detected the H92α line from Arp 220, M83, and NGC 2146. The line was not detected in NGC 6240. Based on these VLA observations and the continuum data obtained from the VLA archives, we have considered two types of models: (1) a collection of H II regions and (2) a uniform slab of ionized gas. In addition, combining previous published data with these new observations, a sample of 13 galaxies has been observed for the H92α line. The H92α line luminosities have also been compared with both the Brα line and the molecular lines of HCN/HCO$^+$. The following conclusions can be drawn from this investigation:

1. The line emission arises from the nuclear regions with a line-to-continuum ratio of 1% or less and FWHM line widths of 100–350 km s^{-1}.

2. With electron temperature in the range of 5×10^3–5×10^4 K and a range of electron densities, the collective H II region model can account for both the observed line intensity and the continuum spectrum. In most cases, the H92α line is dominated by internal stimulated emission due to the free-free continuum emission arising within the H II regions. In a low-density model appropriate for Arp 220, about half the line emission comes from external stimulated emission due to the background nonthermal source.

3. A model with two components with different densities is employed to fit both the line and continuum data of NGC 2146. One hundred compact H II regions with very high density ($n_e = 1 \times 10^5$ cm^{-3}, $T_e = 5000$ K, and size of 0.2 pc) are required for the line intensity observed at 43 GHz, while a few hundred lower density H II regions ($n_e = 5 \times 10^3$–1×10^4 cm^{-3}, $T_e = 5000$–7500 K, and size of 1 pc) may be responsible for the line emission at centimeter wavelengths. This high-density component is highly non-LTE, and the H$n\alpha$ lines at millimeter wavelengths are primarily due to internal stimulated emission.

4. The H92α line flux density and the continuum spectrum in Arp 220 can be fitted by either a low-density, higher temperature thick slab or a high density, lower temperature thin slab. Further observations of H$n\alpha$ are required in order to constrain the model better. In the slab models, the stimulated line emission is dominant at low frequencies and the external stimulated line emission due to the thermal dust radiation appears to be insignificant at millimeter wavelengths because both the line and continuum optical depths are small. Slab models with $T_e = 5000$ K are applicable to M83. There are no uniform slab models with $T_e \geq 5 \times 10^3$ K that fit the data of NGC 2146.

5. The H92α line luminosity appears to be correlated with the Brα line luminosity. We find also a significant excess in the H92α line compared to the expected LTE value. The excess suggests that non-LTE effects are important for the H92α line in these starburst nuclei.

6. We find also a strong correlation between H92α and the dense molecular lines of HCN/HCO$^+$. This correlation suggests that the average electron density of the H II regions emitting RRLs could be as high as the dense molecular medium ($n_e > 10^4$ cm^{-3}). Since the HCN/HCO$^+$ line emission traces the dense molecular cores and the H92α line emission arises primarily from H II regions associated with young massive stars, the correlation may imply the presence of massive star formation within the dense molecular cores in these starburst nuclei.

We thank Alan Roy for critical comments. We also thank the anonymous referee for valuable comments. J. H. Z. thanks the ASIAA for its hospitality. This research was supported in parts by NSC 85-2816-M001-006L of Taiwan.

REFERENCES

Anantharamaiah, K. R., & Goss, W. M. 1990, in IAU Colloq. 125, Radio Recombination Lines: 25 Years of Investigation, ed. M. A. Gordon & R. L. Sorochenko (Dordrecht: Kluwer), 267
Anantharamaiah, K. R., Zhao, J.-H., Goss, W. M., & Viallefond, F. 1993, ApJ, 419, 585 (Paper I)
Baan, W. A., van Gorkom, J. H., Schmelz, J. T., & Mirabel, I. F. 1987, ApJ, 313, 102
Baan, W. A., Wood, P. A. D., & Haschick, A. D. 1982, ApJ, 260, L49
Becklin, E. E., Matthews, K., Neugebauer, G., & Willner, S. 1978, ApJ, 220, 831
Becklin, E. E., & Wynn-Williams, C. G. 1987, in Proc. Star Formation in Galaxies, Conf. (Pasadena: JPL), 643
Carral, P., Turner, J. L., & Ho, P. T. P. 1990, ApJ, 362, 434
Cornwell, T. J., Uson, J. M., & Haddad, N. 1992, A&A, 258, 583
Cowan, J. J., & Branch, D. 1985, ApJ, 293, 400
Crawford, M. K., Genzel, R., Townes, C. H., & Watson, D. M. 1985, ApJ, 291, 755
Depoy, D. L., Becklin, E. E., & Geballe, T. R. 1987, ApJ, 316, L63
Depoy, D. L., Becklin, E. E., & Wynn-Williams, C. G. 1986, ApJ, 307, 116
Diamond, P. J., Norris, R. P., Baan, W. A., & Booth, R. S. 1989, ApJ, 340, L49
Eales, S. A., Becklin, E. E., Hodapp, K.-W., Simons, D. A., & Wynn-Williams, C. G. 1990, ApJ, 365, 478
Eales, S. A., Wynn-Williams, C. G., & Duncan, W. D. 1989, ApJ, 339, 859
Emerson, J. P., Clegg, P. E., Gee, G., Cunningham, C. T., Griffin, M. J., Brown, L. M. J., Robson, E. I., & Longmore, A. J. 1984, Nature, 311, 237
Fabbiano, G., Heckman, T., & Keel, K. C. 1990, ApJ, 355, 442
Feigelson, E. D., & Berg, C. J. 1983, ApJ, 269, 400
Fisher, J. R., & Tully, R. B. 1976, A&A, 53, 397
Graham, J. R., Cario, D. P., Matthews, K., Neugebauer, G., Soifer, B. T., & Wilson, T. D. 1990, ApJ, 354, L5
Handa, T., Nakai, N., Sofue, Y., Hayashi, M., & Fujimoto, M. 1990, PASJ, 42, 1
Ho, P. T. P., Beck, S. C., & Turner, J. L. 1990, ApJ, 349, 57
Hutchings, J. B., Neff, S. G., Stanford, S. A., Lo, E., & Unger, S. W. 1990, AJ, 100, 60
Isobe, T., Feigelson, E. D., & Nelson, P. I. 1986, ApJ, 306, 490
Jackson, J. M., & Ho, P. T. P. 1988, ApJ, 324, L5
Joy, M., Lester, D. F., Harvey, P. M., & Frueh, M. 1986, ApJ, 307, 110
Kawara, K., Nishida, M., & Phillips, M. M. 1989, ApJ, 337, 230
Kronberg, P. P., & Biermann, P. 1981, ApJ, 243, 89
Lonsdale, J. C., Diamond, P. J., Smith, H. E., & Lonsdale, C. S. 1994, Nature, 370, 117
Mauersberger, R., Henkel, C., Wilson, T. J., & Harju, J. 1989, A&A, 226, L5
Mirabel, I. F. 1982, ApJ, 260, 75
Norris, R. P. 1988, MNRAS, 230, 345
Nguyen-Q-Rieu, Jackson, J. M., Henkel, C., Truong-Bach, & Mauersberger, R. 1992, ApJ, 399, 521
Ondrechen, M. P. 1985, AJ, 90, 1474
Osterbrock, P. E. 1989, Astrophysics of Gaseous Nebulae and Active Galactic Nuclei (Mill Valley: Univ. Science Books)
Puxley, P. J., Brand, P. W. J. L., Moore, T. J. T., Mountain, C. M., & Nakai, N. 1991, MNRAS, 248, 585
Radford, S. J. E., et al. 1991, in Dynamics of Galaxies and Their Molecular Cloud Distributions, ed. F. Combes & F. Casoli (Dordrecht: Kluwer), 303
Rickard, L. J., Palmer, P., Morris, M., Turner, B. E., & Zuckerman, B. 1977, ApJ, 213, 673
Rieke, G. H., Lebofsky, M. J., & Walker, C. E. 1988, ApJ, 325, 679
Roelfsema, P. R., & Goss, W. M. 1992, A&A, Rev., 4, 161
Ruiz, M., Rieke, G. H., & Schmidt, G. D. 1994, 423, 608

Sanders, D. B., & Mirabel, I. F. 1985, ApJ, 298, L31
Sanders, D. B., et al. 1988, ApJ, 325, 74
Scoville, N., Sargent, A. I., Sanders, D. B., & Soifer, B. T. 1991, ApJ, 366, L5
Seaquist, E. R., Kerton, C. R., & Bell, M. B. 1994, ApJ, 429, 612
Shaver, P. A. 1978, A&A, 68, 97
Solomon, P. M., Downes, D., & Radford, S. J. E. 1992, ApJ, 387, L55
Solomon, P. M., Radford, S. J. E., & Downes, D. 1990, ApJ, 348, L53
Solomon, P. M., & Sage, L. J. 1988, 334, 613
Turner, J. L., Ho, P. T. P., & Beck, S. C. 1987, ApJ, 313, 644
Wang, Z., Scoville, N. Z., & Sanders, D. B. 1991, ApJ, 368, 112
Woody, D. P., Scott, S. L., Scoville, N. Z., Mundy, L. G., Sargent, A. I., Padin, S., Tinney, C. G., & Wilson, C. D. 1989, ApJ, 337, L41
Young, J. S., Claussen, M. J., Kleinmann, S. G., Rubin, V. C., & Scoville, N. 1988, ApJ, 331, L81
Zhao, J.-H., et al. 1996, in preparation